Improvements to an Empirical Parameterization of Heterogeneous Ice Nucleation and Its Comparison with Observations

VAUGHAN T. J. PHILLIPS,* PAUL J. DEMOTT,+ CONSTANTIN ANDRONACHE,# KERRI A. PRATT,@,++ KIMBERLY A. PRATHER,@ R. SUBRAMANIAN,& AND CYNTHIA TWOHY**

* *School of Earth and Environment, University of Leeds, Leeds, United Kingdom*
+ *Department of Atmospheric Science, Colorado State University, Fort Collins, Colorado*
# *Boston College, Chestnut Hill, Massachusetts*
@ *Department of Chemistry and Biochemistry, University of California, San Diego, La Jolla, California*
& *Droplet Measurement Technologies, Boulder, Colorado*
** *College of Oceanic and Atmospheric Sciences, Oregon State University, Corvallis, Oregon*

(Manuscript received 9 March 2012, in final form 27 August 2012)

ABSTRACT

A framework for an empirical parameterization (EP) of heterogeneous nucleation of ice crystals by multiple species of aerosol material in clouds was proposed in a 2008 paper by the authors. The present paper reports improvements to specification of a few of its empirical parameters. These include temperatures for onset of freezing, baseline surface areas of aerosol observed in field campaigns over Colorado, and new parameters for properties of black carbon, such as surface hydrophilicity and organic coatings. The EP's third group of ice nucleus (IN) aerosols is redefined as that of primary biological aerosol particles (PBAPs), replacing insoluble organic aerosols. A fourth group of IN is introduced—namely, soluble organic aerosols.

The new EP predicts IN concentrations that agree well with aircraft data from selected traverses of shallow wave clouds observed in five flights (1, 3, 4, 6, and 12) of the 2007 Ice in Clouds Experiment–Layer Clouds (ICE-L). Selected traverses were confined to temperatures between about −25° and −29°C in layer cloud without homogeneously nucleated ice from aloft. Some of the wave clouds were affected by carbonaceous aerosols from biomass burning and by dust from dry lakebeds and elsewhere. The EP predicts a trend between number concentrations of heterogeneously nucleated ice crystals and apparent black carbon among the five wave clouds, observed by aircraft in ICE-L. It is predicted in terms of IN activity of black carbon.

The EP's predictions are consistent with laboratory and field observations not used in its construction, for black carbon, dust, primary biological aerosols, and soluble organics. The EP's prediction of biological ice nucleation is validated using coincident field observations of PBAP IN and PBAPs in Colorado.

1. Introduction

Indirect effects on climate from particulate air pollution ("aerosol pollution"), by altering warm clouds, account for most of the uncertainty about the net forcing of climate change. A rare minority of such aerosol particles can nucleate ice. Hence, there is a need to quantify cold-cloud indirect effects too (Ramanathan et al. 2001). But first, the linkage between aerosol conditions and ice numbers must be quantified reliably. In 2007, the Intergovernmental Panel on Climate Change (IPCC; Forster et al. 2007) claimed that knowledge of ice nucleation by aerosol species was too scarce for any assessment of cold-cloud indirect effects. Since then there has been a resurgence of observations about ice nucleation (DeMott et al. 2011, hereafter D11).

A flexible framework—namely, an empirical parameterization (EP)—for treating heterogeneous ice nucleation by chemical species of aerosol was proposed by Phillips et al. (2008, hereafter Ph08). It was designed to be versatile so as to assimilate new observations of ice nucleus (IN) activity that would arise in the future literature. Since 2008, some laboratory data, such as those suggesting approximate proportionality between the concentration of active IN and total surface area of IN aerosols (Welti et al. 2009; Niemand et al. 2012, hereafter N12),

++ Current affiliation: Department of Chemistry, Purdue University, West Lafayette, Indiana.

Corresponding author address: Vaughan T. J. Phillips, School of Earth and Environment, University of Leeds, Woodhouse Lane, Leeds LS2 9JT, United Kingdom.
E-mail: v.phillips@leeds.ac.uk

DOI: 10.1175/JAS-D-12-080.1

have qualitatively supported assumptions made in the EP's original construction. Compilation of recent laboratory observations by Hoose and Möhler (2012) has corroborated the suppression of ice nucleation by dust at humidities below water saturation for warm subzero temperatures, as assumed by Ph08.

Moreover, Vali (2008) observed random variations of only about 0.2°C in the freezing temperature of each drop of soil suspension in successive cycles of cooling. It corroborated observations by Shaw et al. (2005). This is consistent with the validity of the ''modified singular'' approximation, assumed for IN measurements with the field probe as the basis for the EP. This approximation assumes that ice nucleation occurs almost instantaneously when any IN particle's characteristic temperature (or humidity) is reached. The freezing probability per unit time is assumed to increase very steeply from almost zero to a high value with supercooling (Vali 2008). The modified singular approximation was seen to be valid for Arizona Test Dust (ATD) by Marcolli et al. (2007), who simulated the stochastic behavior of rare but very efficient ''active sites'' for ice nucleation on the dust surface. However, it seems less applicable to pure mineral compounds. The relaxation time τ of the active fraction of pure kaolinite was seen to be constant over time according to a simple exponential law (Murray et al. 2011, their Fig. 3). The time scale depended on temperature and size, ranging from about 1 min to 1 h (see also Welti et al. 2012).

Illite-rich dust is less pure and hence more representative for the atmosphere. It was seen to have an active fraction increasing quickly initially but much more slowly later during each isothermal experiment (Broadley et al. 2012, their Figs. 7a and 12). Effectively there was a dramatic lengthening of τ over time during each experiment, making the modified singular approximation more applicable. Broadley et al. (2012) and Niedermeier et al. (2011, their Fig. 7b) explained such behavior in terms of widely varying efficiencies of multiple sites on each IN particle due to lack of purity. For ATD at constant temperature, the active fraction after 10 min was only about twice that found after 10 s. It again involved a growth of τ during each experiment. For IN activity, a factor of 2 is a small difference. Although some laboratory observations of mineral dust showed $\tau \sim 1$ min (Kulkarni and Dobbie 2010), those by Connolly et al. (2009) and Niedermeier et al. (2011) were fitted adequately by a model with the singular approximation.

Nevertheless, regarding the activity of particular aerosol species, the most recent laboratory observations have changed perspectives in some ways. Certain types of black carbon (e.g., hydrophobic soot) were seen to be very poor at nucleating ice (Koehler et al. 2009, hereafter K09; Crawford et al. 2011, hereafter C11). IN activity is now seen to be scarce in carbonaceous plumes freshly emitted from fossil-fuel combustion, which the original version of the EP would have overpredicted with too many insoluble organic and soot IN. Copious IN activity was seen in some, but not all, samples of biomass-burning particles from diverse plumes (Petters et al. 2009a). Soluble organic IN have been estimated to be potentially prolific in the upper troposphere (Murray et al. 2010, hereafter Mu10)—an apparent group of IN that the original version of the EP missed. This is not yet proven, however. Recent studies of biological ice nucleation have increased awareness of the fact that different species of IN have different temperatures of onset of measurable ice nucleation in the laboratory. This variability was not treated by the original version of the EP. Such onset temperatures have been measured more accurately very recently (e.g., Connolly et al. 2009; D11; N12). Hence, the original EP overpredicted IN concentrations by at least an order of magnitude at temperatures warmer than −20°C in the comparison by N12.

Consequently, in the present paper the EP is revised so as to align it better with observations of IN activity, including those made since 2008. The EP's treatment of deposition and condensation-/immersion-freezing modes was formulated originally by Ph08 as

$$n_{\mathrm{IN},X} = \int_{\log(0.1\mu\mathrm{m})}^{\infty} \{1 - \exp[-\mu_X(D_X, S_i, T)]\} \frac{dn_X}{d\log D_X} d\log D_X \quad \text{and} \tag{1}$$

$$\mu_X = H_X(S_i, T)\xi(T)\left(\frac{\alpha_X n_{\mathrm{IN},1,*}}{\Omega_{X,1,*}}\right) \times \frac{d\Omega_X}{dn_X} \quad \text{for} \quad T < 0°\mathrm{C} \quad \text{and} \quad 1 < S_i \le S_i^w. \tag{2}$$

Here, $n_{\mathrm{IN},X}(S_i, T)$ is the number mixing ratio of IN activated at a saturation ratio with respect to ice S_i and temperature T in the Xth species; $S_i^w(T)$ is the value of S_i at water saturation; Ω_X is the total surface area of all insoluble aerosol cores with dry diameters D_X larger than 0.1 μm, per unit mass of air (the ''surface area mixing ratio'') in group X; and $d\Omega_X/dn_X \approx \pi D_X^2$. The groups were originally defined as mineral dust–metallic

aerosols (X = DM), black carbon (X = BC), and insoluble organics ($X = O$). The quantities Ω_X and n_X are "ideal," as they are not depleted while in cloud by nucleation of ice or liquid. The μ_X is the average number of potentially activated ice embryos per insoluble aerosol particle of size D_X and their areal density ($\mu_X/\pi D_X^2$) is uniform over all D_X. If $S_i > S_i^w$, then $\mu_X(S_i, T) = \mu_X(S_i^w, T)$ and freezing is assumed to be insensitive to humidity above water saturation. The term $\Omega_{X,1,*}$ is the component of Ω_X for aerosol cores with diameters between 0.1 and 1 μm in the "background-troposphere scenario" consisting of field campaigns of the First and Second Ice Nuclei Spectroscopy Studies (INSPECT-1 and -2) (Ph08). The $n_{\mathrm{IN},1,*}$ is the total concentration of active IN of all species measured during INSPECT-1 and -2, normalized to water saturation. During this scenario's campaigns, the continuous flow diffusion chamber (CFDC) (Rogers et al. 2001) measurements of IN underpinning the EP's construction were made. In Eq. (2), $H_X(S_i, T)$ is an empirically determined fraction ($0 \le H_X \le 1$) representing the scarcity of heterogeneous nucleation of ice seen in substantially water-subsaturated conditions. The quantity H_X was expressed by Ph08 in terms of a parameter $f_C(S_i, T)$. At water saturation, $H_X = 1$. In the background-troposphere scenario, α_X is the fractional contribution from aerosol group X to the IN concentration (when $H_X = 1$) inferred from CFDC data.

The quantity ξ accounts for laboratory observations that drops are seen not to freeze at temperatures warmer than a threshold. Originally, Ph08 proposed $\xi = \delta_1^0(T, T_1, T_2)$, which is 1 for $T < T_1$ and 0 for $T > T_2$, with an interpolation in between (appendix A). Ph08 assumed T_1 (−5°C) and T_2 (−2°C) were the same for all aerosol species X. Such temperature thresholds are required to prevent unrealistic extrapolation of the field data for IN activity to warm temperatures, where active IN are rare and difficult to measure with field probes.

Equation (1), when $\mu_X \ll 1$, expresses a proportionality between active IN concentrations and the total surface area of aerosols in each species, as seen in observations (e.g., Welti et al. 2009). It is integrated numerically: $n_{\mathrm{IN},X} \approx \sum_{j,(D_{X,j}>0.1\mu\mathrm{m})}^{\infty}\{1 - \exp[-\mu_X(D_{X,j}, S_i, T)]\}\Delta n_{X,j}$, where $\Delta n_{X,j}$ is the element of n_X in the jth bin, $\Delta \log D_{X,j}$. For a bulk aerosol treatment, the grid of size bins is temporary and $\Delta n_{X,j}$ is diagnosed from prognostic variables for the ideal amount of aerosol.

It is easy to adapt Eq. (1) for a model with a bin treatment of aerosols; $\Delta n_{X,j}$ would then become a prognostic variable, of which a fraction, $1 - \exp[-\mu_X(D_{X,j}, S_i, T)]$, is active. Those lost by activation in each bin would be counted.

Outside-in and inside-out contact freezing were treated with the EP of Ph08 by assuming each IN particle activates in either the immersion or contact-freezing mode, with a difference in activation temperature of $\Delta T_{\mathrm{CIN}} = 4.5$ K. Assuming $\mu_X \ll 1$, the number mixing ratio of potentially active contact-freezing IN (CIN) that are interstitial was originally

$$n_{X,\mathrm{cn}} \approx \alpha_X \xi(T)\left\{\frac{n_{\mathrm{IN},1,*}[T - \Delta T_{\mathrm{CIN}}, S_i^w(T - \Delta T_{\mathrm{CIN}})]}{\Omega_{X,1,*}}\right\} \times \Omega_{X,\mathrm{int}}, \quad (3)$$

while $\Omega_{X,\mathrm{int}}$ is the interstitial component of Ω_X.

Observations supported the original EP as follows. Firstly, there were three strands of coincident observations of the background troposphere during the INSPECT field campaign at Storm Peak Laboratory (SPL) in 2001 and 2004 on Mt. Werner in Colorado:

- Total concentrations of active IN were measured with the CFDC in the background troposphere at temperatures between −40° and −62°C during INSPECT-1 (DeMott et al. 2003a) and -2 (Richardson et al. 2007). This yielded $n_{\mathrm{IN},1,*}$. Dependencies of IN activity observed with the CFDC from Meyers et al. (1992) were used to extrapolate the IN activity at SPL to temperatures as warm as −7°C.
- Surface area mixing ratios of dust, soot, and insoluble organic species during INSPECT at SPL, $\Omega_{X,1,*}$, were inferred from measurements. For dust, optical probes deployed there provided the data. For carbonaceous material, the data was from the Interagency Monitoring for Protection of Visual Environments (IMPROVE) at Mt. Zirkel nearby.
- Relative contributions (α_X) from dust, soot, and insoluble organics to the total IN concentration at SPL were estimated from composition fractions observed during INSPECT and previous field campaigns in the background troposphere. Residual material was collected from ice crystals sampled from the troposphere under conditions of heterogeneous freezing. The analysis of its composition involved transmission electron microscopy energy dispersive X-ray spectral analysis (TEM-EDS) (Ph08, their Fig. 2). Since insoluble organics [e.g., primary biological aerosol particles (PBAPs)] were not resolved by measurements at INSPECT, other field and laboratory observations of bacterial abundance and IN activity were used to distinguish their contribution from that of soot.

They were combined to provide a measure of the activity spectrum of the Xth species normalized by aerosol surface area at water saturation—namely, $\alpha_X n_{\mathrm{IN},1,*}(T)/\Omega_{X,1,*}$. Second, extra observations of nucleation in subsaturated conditions have been combined

with the spectrum by means of $H_X(S_i, T)$. IN activity can then be predicted for all humidities.

A full description of the original version of the EP and its validation and implementation with discussion of underlying assumptions, are given by Ph08. The extended set of all CFDC field measurements of active IN concentrations underpinning the EP ranged from −7° to −62°C and over most humidities between ice and water saturation. The assumed proportionality between aerosol surface area and IN number, noted above, made the EP applicable to a wide range of mean sizes, chemistry, and loadings of aerosol. Hence, the EP applies to most subzero temperatures, humidities, and aerosol conditions throughout the global troposphere.

In the next section, the improvements to the EP are described. These are informed by recent laboratory and field experiments. The most pivotal aspect of the upgraded EP—namely, $\alpha_X n_{\mathrm{IN},1,*}(T)/\Omega_{X,1,*}$ is still constrained by the coincident observations of IN and aerosols from INSPECT noted above. A more accurate analysis of this INSPECT data is provided here, to infer better values for baseline surface areas, $\Omega_{X,1,*}$. New onsets, and differences between modes, for temperatures of freezing are given. Dependencies of soot's IN activity on its properties are introduced. The identity of IN species is revisited. In subsequent sections, the revised EP is then compared with laboratory and aircraft observations. There is a summary of the changes and results in the concluding section.

2. Modifications to the EP

a. Thresholds at warm temperatures for the onset of heterogeneous ice nucleation by condensation/immersion freezing

The factor ξ in Eq. (2) represented the onset of measurable heterogeneous freezing during supercooling at warm temperatures in the original EP. It made all freezing for all species start at about −2°C. That assumption is altered as follows to treat the observed dependency on aerosol species of the onset temperature.

1) DUST/METALLIC GROUP OF IN (X = DM)

Recent CFDC observations of the IN activity of submicron dust particles suspended from a Saharan soil sample indicate that these activate in sparingly smaller fractions at warmer subzero temperatures, reaching 1 IN in 10^5 particles at about −15°C (D11). This is consistent with laboratory observations of various types of surrogate dust with onset temperatures ranging from about −10° to −15°C (e.g., Mason and Maybank 1958; Roberts and Hallett 1968; Pitter and Pruppacher 1973, hereafter PP73). They are reviewed by Pruppacher and Klett (1997, hereafter PK97). Surrogate particles (1–10 μm) of pure minerals (e.g., kaolinite, illite) were seen to have temperatures of between about −10° and −16°C for active fractions of 1% in the deposition mode (Zimmermann et al. 2008). Freezing by freshly emitted Saharan dust over Germany was measured at −18°C, so its onset temperature was warmer than this (Klein et al. 2010).

Yet colder onset temperatures for ice nucleation have been seen in the Aerosol Interaction and Dynamics in the Atmosphere (AIDA) chamber. Saharan (SD2) and Asian (AD1) surrogate submicron dust nucleated ice at fractions greater than 1 IN in 10^4 only at temperatures colder than about −24° and −18°C, respectively (Connolly et al. 2009), and about −19°C by D11 for SD2 via multiple instruments. This extended other AIDA observations by Field et al. (2006, hereafter F06) to warmer temperatures. Differences in composition (e.g., Gallavardin et al. 2008) and size (e.g., Welti et al. 2009) of dust particles may explain such variability.

Some field measurements exist suggesting that some atmospheric dusts may be active at temperatures warmer than −10°C (Sassen et al. 2003). However, the relative frequency of occurrence of such activity and associated active fractions remains to be shown. Ansmann et al. (2008) did not see it, remotely observing ice in clouds with tops colder, but not warmer, than −15°C in dusty conditions. When copious dust is seen to coincide with nucleation of ice at temperatures warmer than −10°C, this could also be due to activity of other IN material accreted onto the dust. For instance, primary biological material can be active at very warm temperatures and fragments of it may stick to the surface of natural atmospheric dust (Schnell and Vali 1976; Griffin et al. 2001). Organic content from decayed vegetation also yields IN (Schnell and Vali 1972). This might coexist with airborne dust. Alternatively, either preactivation of some dust (Mason and Maybank 1958; Roberts and Hallett 1968) at temperatures as warm as −5°C or its contact freezing (see section 2d), followed by ice multiplication, might be at play in the observations by Sassen et al. (2003).

2) BLACK CARBON GROUP OF IN (X = BC)

For surrogate black carbon made in the laboratory from acetylene, DeMott (1990, hereafter D90) detected ice nucleation at temperatures colder than about −24°C and humidities above water saturation. Hallett et al. (1986) observed no ice nucleation by flame soot at temperatures warmer than −15°C. This was not an onset temperature.

Diehl and Mitra (1998, hereafter DM98) did observe at about −18°C, an onset of immersion freezing by black

carbon particles from combustion of kerosene. They were between 10 and 1000 nm in size. Yet only frozen fractions of drops were reported. We correct for this as follows. Each (0.8 mm) drop had a total of about $N_s = 90$ black carbon particles on average. Assuming a Poisson distribution of the number φ of active IN in a given (0.8 mm) drop, then the probability of it freezing is $P(\varphi > 0) = 1 - \exp(-\mu^*)$, where μ^* is the population mean of φ for all such drops. From their observations at −20°C, $P(\varphi > 0) = 0.1$ and so the active fraction of the black carbon particles is $\mu^*/N_s \approx 0.1\%$. It is comparable with that seen by D90 for black carbon from acetylene combustion, though the temperature of this onset (0.1%) is about 5 K warmer. In the temperature range of overlap at −24° to −28°C, between observations by D90 and DM98, the active fraction from the latter is higher by a factor of between 1.5 and 10 (section 3b). It has a similar order of magnitude. Popovicheva et al. (2008a) observed ice nucleation by black carbon from kerosene and propane–butane combustion at temperatures as warm as −7°C. Yet the innumerable black carbon particles in each drop were not counted. Their active fraction cannot be inferred.

Much colder onset temperatures for some types of black carbon are possible. For example, Fornea et al. (2009, hereafter F09) observed contact freezing by giant particles (0.2–0.3 mm) of carbon lampblack at −19°C. The observed freezing fraction was ~0.1 between −20° and −25°C. This implies a very low active fraction of $\sim 10^{-7}$ for typical sizes of black carbon of 0.1 μm in the atmosphere, since it is proportional to surface area. Similarly, between −40° and −60°C, artificial black carbon generated by various methods displayed active fractions differing by up to about four orders of magnitude at given conditions (K09). One of the methods was burning of kerosene. All ice nucleation on all types of black carbon observed by K09 was absent at temperatures warmer than about −40°C. Owing to scarcity of laboratory data at such warm temperatures and diversity of black carbon properties, there is much uncertainty.

3) MODIFICATION OF EP

Generally, both dust and black carbon are observed in the laboratory to nucleate ice only at temperatures much colder than for the "most IN active" of PBAPs. In light of the above observations, T_1 and T_2 in the expression for ξ [Eq. (2)] are replaced by species-specific parameters, $T_{X,1}$ and $T_{X,2}$. Their new values are listed in Table 1 (see also appendix A):

$$\xi = \delta_1^0(T, T_{X,1}, T_{X,2}). \quad (4)$$

b. Baseline surface areas of black carbon and dust

In the original version of the EP, Ph08 estimated the baseline surface areas, $\Omega_{X,1,*}$ [Eq. (2)], describing aerosol conditions coincident with the IN activity observed during INSPECT. They are evaluated again more accurately, as follows.

1) DUST/METALLIC GROUP OF IN ($X = DM$)

A baseline value of surface area mixing ratio $\Omega_{\mathrm{DM},1,*}$ was derived by Ph08 from observations of the aerosol size distribution (ASD) during INSPECT-1. Yet the CFDC data of this background-troposphere scenario were from both INSPECT-1 and -2, for measurements of IN concentration that were combined with this baseline value. As aerosol conditions during INSPECT-2 were more dusty than in INSPECT-1, Eidhammer et al. (2010, hereafter E10) included aerosol observations from INSPECT-2 in the averaging for the baseline surface area of dust. E10 proposed $\Omega_{\mathrm{DM},1,*} = 2 \times 10^{-6}$ m^2 kg^{-1}, which is a value four times higher than proposed by Ph08. We agree with this revised value and also adjust the baseline surface area for black carbon similarly, as follows.

2) BLACK CARBON GROUP OF IN ($X = BC$)

INSPECT-2 observations are included here in revised estimates of the baseline surface area mixing ratios $\Omega_{\mathrm{BC},1,*}$. Only INSPECT-1 data were used previously, as with dust. In the present paper, geometric means of all daily values of surface area mixing ratio are derived from observations at the Mt. Zirkel IMPROVE station during INSPECT-1 and -2. The same iterative correction explained by Ph08 (their appendix D) is applied to correct the nominal measurements of elemental and organic carbon on each observational (CFDC) day of INSPECT-1 and -2. It corrects for the contribution to the elemental carbon measurement from refractory organic carbon that remains after the heating cycle in the test to measure elemental carbon content. On days when the mass concentration of sulfate at Mt. Zirkel is less than that of all organic (both soluble and insoluble) mass, then the refractory fraction of organic mass is assumed to be 0.2 for the iterative correction. Otherwise a refractory fraction of 0.3 is assumed. Both fractions are from observations of the Intercontinental Chemical Transport Experiment–North America (INTEX-NA) campaign by Clarke et al. (2007, their Figs. 2 and 3).

3) MODIFICATION OF EP

New baseline values are presented in Table 1 (see appendix A). A more accurate value of 90 nm for the geometric mean diameter of black carbon in the background troposphere is used (Clarke et al. 2004, hereafter

TABLE 1. New and revised parameters for the EP. They include onset temperatures of heterogeneous ice nucleation at water saturation $T_{X,1}$ and $T_{X,2}$ and baseline surface area mixing ratios $\Omega_{X,1,*}$ of insoluble aerosol cores in groups X = DM, BC, BIO, and solO. For $T_{X,\ldots}$, observations from D90, D11, and DM98 were used (see PK97). The quantity $\Omega_{X,1,*}$ for X = DM, BC, BIO is from observations by E10 (a correction), INSPECT-1 and -2 and IMPROVE, and W09, respectively. Geometric mean diameters $D_{g,X}$ and/or dry bulk densities ρ_X are from C04, in the first [second] mode of the PBAP ASD from M95, and also from Matthias-Maser et al. (2000, hereafter M00), Froyd et al. (2009, hereafter Fr09), and Ming et al. (2006, hereafter Mi06). The ratio of total numbers of PBAPs ($n_{\mathrm{BIO},1}$: $n_{\mathrm{BIO},2}$) in both modes and their standard deviation ratios σ_{BIO} are from M95. Temperature shifts between contact- and immersion-freezing modes (full activity: $\Delta T_{\mathrm{CIN},X}$; onset of freezing: $\Delta T_{\mathrm{onset},X}$) are from PP73, Co80, and F09 for dust and from LY83 and CB10 for PBAPs. For black carbon, $F_{\mathrm{OC},\ldots}$ and $P_{s,\ldots}$ are from K09 and from the present paper for ice-nucleating biomass-burning plumes (urban freshly emitted fossil-fuel pollution [FFFP]). All other parameters not listed here are unchanged from Ph08, with those for X = BIO the same as for the previous $X = O$ group.

Adjusted or new variable	New value	Origin
$(D_{g,\mathrm{BC}}, D_{g,\mathrm{BIO}}, D_{g,\mathrm{solO}})$	(90, 163 [466] of first [second] mode, 150) nm	(C04, M95, Fr09/Mu10)
f_C	$\delta_1^{h^X}(T, T_0^X, T_0^X + \delta_T^X)\delta_0^1(S_i, S_{i,0}^X, S_{i,0}^X + \Delta S_i^X)/\gamma$	Section 2c
F_{OC}	≈0 (1) for biomass burning plumes (FFFP)	Section 2e
$(F_{\mathrm{OC},0}, F_{\mathrm{OC},1})$	(0.1, 1)	Section 2e
g_{glass}	0.5	Mu10
$H_{\mathrm{solO}}(S_i, T)$	$\delta_1^0(T, -75°, -65°\mathrm{C}) \times \delta_0^1(S_i, 1.2, 1.3)$	Eq. (9)
$n_{\mathrm{BIO},1}$: $n_{\mathrm{BIO},2}$	347	M95
$n_{\mathrm{IN,solO,@}}$	$10^6 \times (7.7211 S_i - 9.2688)/\rho_@$ kg^{-1} for $1.2 < S_i < S_i^w$	Mu10
P_s	$> P_{s,1}$ ($< P_{s,0}$) for biomass burning plumes (FFFP)	Section 2e
$(P_{s,0}, P_{s,1})$	(1, 2) H_2O monolayers	K09
$S_{i,0}^{\mathrm{BC}}$	$\tilde{S}_{i,0}^{\mathrm{BC}} + \delta_0^1(F_{\mathrm{OC}}, F_{\mathrm{OC},0}, F_{\mathrm{OC},1}) \times [1.2 \times S_i^w(T) - \tilde{S}_{i,0}^{\mathrm{BC}}]$	Section 2e
$\tilde{S}_{i,0}^{\mathrm{BC}}$	1.3	K09, C11, DeMott et al. (1999)
$S_{i,0}^{\mathrm{BIO}}$	1.15	CB10
$(\Delta S_i^{\mathrm{DM}}, \Delta S_i^{\mathrm{BC}}, \Delta S_i^{\mathrm{BIO}})$	(0.1, 0.1, 0.2)	Section 2c, 2e
$(T_{\mathrm{DM},1}, T_{\mathrm{DM},2})$	(−30°, −10°)C	D11, PK97
$(T_{\mathrm{BC},1}, T_{\mathrm{BC},2})$	(−25°, −15°)C	D90, DM98
$(T_{\mathrm{BIO},1}, T_{\mathrm{BIO},2})$	(−5°, −2°)C	Ph08
T_0^{BC}	−50°C	Section 2e
T_0^{BIO}	−20°C	Section 2c
$(\Delta T^{\mathrm{DM}}, \Delta T^{\mathrm{BC}}, \Delta T^{\mathrm{BIO}})$	(5°, 10°, 5°)C	Section 2c, 2e
$(\Delta T_{\mathrm{onset,DM}}, \Delta T_{\mathrm{CIN,DM}})$	(6°, 10°)C	PP73, Co80, F09
$(\Delta T_{\mathrm{onset,BC}}, \Delta T_{\mathrm{CIN,BC}})$	(4.5°, 4.5°)C	Section 2d
$(\Delta T_{\mathrm{onset,BIO}}, \Delta T_{\mathrm{CIN,BIO}})$	(1°, 3°)C	LY83
α_{BC}	$\Xi\tilde{\alpha}_{\mathrm{BC}}$	Section 2e
$\tilde{\alpha}_{\mathrm{BC}}$	1/3 − 0.03	
α_{BIO}	0.03	
ξ	$\delta_1^0(T, T_{X,1}, T_{X,2})$	Eq. (4)
Ξ	$\delta_0^1(P_s, P_{s,0}, P_{s,1}) \times \delta_1^0(F_{\mathrm{OC}}, F_{\mathrm{OC},0}, F_{\mathrm{OC},1}) \approx 1(0)$ for biomass burning plumes (FFFP)	Section 2e
$(\rho_{\mathrm{BIO}}, \rho_{\mathrm{solO}}, \rho_@)$	(1000, 1360, 1.530) kg m^{-3}	(M00, Mi06, Mu10)
$(\sigma_{\mathrm{BIO}}, \sigma_{\mathrm{solO}})$	(2.54 [3.96] of first [second] mode, 1.4) nm	(M95, Fr09/Section 3a)
$(\Omega_{\mathrm{DM},1,*}, \Omega_{\mathrm{BC},1,*}, \Omega_{\mathrm{BIO},1,*})$	$(2.0 \times 10^{-6}, 1 \times 10^{-7}, 8.9 \times 10^{-7})$ m^2 kg^{-1}	E10, INSPECT, W09
$\Omega_{\mathrm{solO},@}$	5.6×10^{-5} m^2 kg^{-1}	Mu10

C04) to derive its baseline surface area. This new value (90 nm) is to be used with the EP whenever the mean size of black carbon cannot be predicted or observed. All other parameters of ASDs of black carbon and dust for the background troposphere are as specified by Ph08.

c. *New group for primary biological aerosol (X = BIO) replaces $X = O$ group*

In the original version of the EP, PBAPs' nucleating ability was assumed by Ph08 to be representative for all insoluble organics. That assumption is changed here, with introduction of a new group specifically for PBAP IN.

In the original scheme the suppression of ice nucleation at humidities below water saturation was treated by the factor H_X which was expressed in terms of another parameter $f_C(S_i, T)$ [Ph08, their Eqs. (11)–(12)]. Ranges of humidity and temperature, over which the onset of nucleation occurs during humidification and supercooling, had constant values: ΔS_i and ΔT in the original expression for f_C. Now species-specific values, ΔS_i^X and ΔT^X, replace ΔS_i and ΔT. Threshold values of

humidity and temperature in H_X—namely, $S_{i,0}^X$ and T_0^X—for ice nucleation at humidities well below water saturation are also changed for black carbon (section 2e) and the new primary biological group.

1) RECENT OBSERVATIONS

Field studies over the Amazon (Prenni et al. 2009), Wyoming (Pratt et al. 2009a), and the area of Colorado and Nebraska (Bowers et al. 2009; Garcia et al. 2012) suggest that PBAPs act as IN. Over the Amazon, PBAPs are abundant and some act as IN, dominating ice nucleation at temperatures warmer than −25°C (Prenni et al. 2009). This is consistent with a long history of laboratory observations of ice nucleation by PBAPs such as bacteria, pollen, and leaf litter (e.g., Maki et al. 1974; Schnell and Vali 1976; Vali et al. 1976; Lindow 1982; Lindow et al. 1982; Levin and Yankofsky 1983, hereafter LY83; Lindow et al. 1989). It is reviewed by Morris et al. (2004) and Möhler et al. (2007).

There is little evidence from laboratory or field (e.g., Cziczo et al. 2004) studies for those insoluble organic species that are not PBAPs acting as IN at warm subzero temperatures. Their molecular lattice may be amorphous (e.g., Virtanen et al. 2010) with poor ice-nucleating ability. Glassy solid particles of soluble organics are not PBAPs yet nucleate ice, but this was only seen by Mu10 at extreme temperatures colder than about −65°C. An organic IN source from decomposing vegetation has been observed (Schnell and Vali 1972; Conen et al. 2011). Its precise composition is not identified yet. Predominantly organic particles from fresh urban fossil-fuel pollution were seen by Knopf et al. (2010) to nucleate ice in the freezing mode at temperatures colder than about 230 K. Yet it is unclear which species in the sampled urban particles really nucleated the ice observed. Also, C11 observed that organic coatings inhibit the IN activity of black carbon at −45°C (see also Möhler et al. 2005b). These coatings partly consisted of insoluble organic material.

This points to a deficiency in the previous version of the EP. The IN could be overpredicted in situations dominated by insoluble organics of aerosol pollution from fresh fossil-fuel combustion (''fossil-fuel pollution'').

2) MODIFICATION OF EP

Consequently, a new aerosol group specifically for organic PBAPs, X = BIO, is introduced to replace the insoluble organic group (X = O). The input for the EP's treatment of this group becomes the ideal size distribution of PBAP cores with diameters >0.1 μm, $dn_{\rm BIO}/d\log D_{\rm BIO}$, or simply $\Omega_{\rm BIO}$, their ideal surface area.

Accordingly, $\Omega_{\rm BIO,1,*}$, the baseline value (INSPECT) of surface area mixing ratio of all PBAPs between 0.1 and 1 μm in diameter replaces $\Omega_{\rm O,1,*}$. Its value is estimated from field observations at the same location and mostly a similar month as INSPECT, albeit from a more recent year, in appendix B.

Originally, $\alpha_{\rm O}$ was estimated by Ph08 (0.06) from measurements of bacterial IN. It is replaced by $\alpha_{\rm BIO} \approx 0.03$.

This approach to modeling biological ice nucleation does not resolve the individual types of PBAP IN, which vary in ice-nucleating ability. They may vary widely in relative abundance geographically and between seasons. Our approach is justified because few atmospheric models can resolve the different types of PBAP. Besides, their ice-nucleating abilities have not been comprehensively measured yet in laboratory studies.

For IN activity at subsaturated humidities well below water saturation, parameters of $H_{\rm BIO}$ appearing in the expression for f_C (appendix A) are changed, relative to $H_{\rm O}$, to account for laboratory observations of ice-nucleating bacterial cells. These are, namely, $S_{i,0}^{\rm BIO}$ and $T_0^{\rm BIO}$. Chernoff and Bertram (2010, hereafter CB10) observed in a flow cell the ice nucleation by an artificial strain (''Snowmax'') of Pseudomonas syringae (Ps) bacteria at about −27°, −31°, and −37°C. They observed an onset of ice nucleation at about $S_i \approx 1.15$, as the humidity increased on time scales of tens of minutes in all three experiments. A similar onset for Snowmax at $S_i = 1.20$ was observed by Kanji et al. (2011) at −26°C. D11 observed Snowmax nucleating ice at −10°C with an onset at 96% relative humidity with respect to water ($S_i = 1.06$). However, this onset of ice nucleation at subsaturated humidities so close to water saturation is already treated by a different parameter not changed here, in $H_{\rm BIO}$. Thus, a conservative estimate is $S_{i,0}^{\rm BIO} = 1.15$. The transition for the onset is assumed to occur over a broad range of humidities $\Delta S_i^{\rm BIO} = 0.2$ in view of the uncertainty from the paucity of experimental data at low humidities and cold temperatures. Since exact water saturation at −15°C has the same humidity as that threshold (1.15), we assign $\Delta T^{\rm BIO} = 5$°C (replaces ΔT in expression for H_X from Ph08) and $T_0^{\rm BIO} = -20$°C. Finally, PBAPs are assumed not to be coated by any nonbiological insoluble organic material.

Parameters for the new PBAP-IN group, such as $\Omega_{\rm BIO,1,*}$ and $S_{i,0}^{\rm BIO}$, are listed in Table 1 (appendix A). Parameters of PBAPs' ASD may be prescribed accordingly if they cannot be predicted. Certain parameters of the PBAP-IN group, such as the temperature thresholds for the onset of freezing at water saturation ($T_{\rm BIO,1} = -5$ and $T_{\rm BIO,2} = -2$°C), have values unchanged from those for the previous insoluble organic group noted by Ph08.

d. Temperature shifts to treat contact freezing and its onset

Originally, Ph08 assumed that the onset of potential contact freezing during supercooling is the same as for other modes of ice nucleation, representing it by ξ [Eq. (4)]. Contact freezing was treated by assuming a constant temperature difference $\Delta T_{\rm CIN}$ between the characteristic temperatures of activation in contact and condensation-/immersion-freezing modes for each IN particle. Any dependencies of $\Delta T_{\rm CIN}$ were neglected.

Yet, in reality, for individual IN particles, $\Delta T_{\rm CIN}$ may depend on composition (e.g., Gokhale and Goold 1968). So, it is now replaced by $\Delta T_{{\rm CIN},X}$ (>0). Also, the temperature of onset of contact freezing is warmer than that of immersion freezing for a given IN species (see PP73) during supercooling from 0°C. The original EP assumed both onsets are the same [see Eqs. (2) and (3)]. Hence, a new temperature shift of $\Delta T_{{\rm onset},X}$ (>0) is introduced into the input for ξ [Eq. (4)] to treat this onset of contact freezing. Replacing Eq. (3) is

$$n_{X,{\rm cn}} \approx \alpha_X \xi(T - \Delta T_{{\rm onset},X}) \times \left\{ \frac{n_{{\rm IN},1,*}[T - \Delta T_{{\rm CIN},X}, S_i^w(T - \Delta T_{{\rm CIN},X})]}{\Omega_{X,1,*}} \right\} \times \Omega_{X,{\rm int}}. \quad (5)$$

Each new temperature shift, $\Delta T_{{\rm CIN},X}$ or $\Delta T_{{\rm onset},X}$ (defined in appendix A), is assumed to be the same for inside-out contact freezing as for outside-in contact freezing. The same assumption was made by Ph08.

Paradoxically, no temperature difference between contact and bulk-liquid modes was seen for a drop freezing on atomically smooth silicon (Gurganus et al. 2011). The difference was 4–5 K for a giant rough particle in a drop (Durant and Shaw 2005; Shaw et al. 2005). The reason for the discrepancy is unclear. The liquid surface accommodates ice volume and has electric fields orienting molecules, and so is favored for homogeneous freezing (Vrbka and Jungwirth 2006). For heterogeneous freezing, geometry of solid and liquid surfaces may be important. Contact freezing seen by Durant and Shaw (2005) and Shaw et al. (2005) might have been favored because of solid roughness, which could have allowed solid contact with the liquid surface away from the line.

A spurious temperature lag in drops from the cooling rate might have caused contact freezing to seem preferred in past experiments (Gurganus et al. 2011). Yet for Durant and Shaw (2005) and Shaw et al. (2005) freezing always started near the cold substrate, where any lag was minimal. F09, without this bias (Gurganus et al. 2011, their Fig. 2), corroborated observations by Durant and Shaw (2005) and Shaw et al. (2005). Some early laboratory studies (e.g., PP73) used slow cooling rates (see below), minimizing the bias. Finally, Durant and Shaw (2005) and Shaw et al. (2005) studied more realistic material for aerosols than Gurganus et al. (2011). This suggests $\Delta T_{{\rm CIN},X} > 0$ for atmospheric IN.

1) DUST/METALLIC GROUP OF IN (X = DM)

F09, Durant and Shaw (2005), and Shaw et al. (2005) observed a difference of 7° and 4°–5°C, respectively, between activation temperatures of contact and immersion freezing by each silicate-containing volcanic-ash particle (>0.1 mm). Gokhale and Goold (1968) reported that this difference is about 5°C for onset of freezing by clay particles (5–10 μm) and by volcanic ash. The difference was overestimated by only 1 K, owing to their choice of cooling rate.

For clay particles of kaolinite and montmorrillonite (0.1–30 μm), observations by PP73 with a wind tunnel show a difference between contact and immersion freezing of 10° (near freezing onset) to 14°C (all drops frozen). This is for a given fraction of drops frozen. Onsets of contact and immersion freezing for montmorrillonite were seen at about −4° and −14°C, respectively. PP73 used slow cooling rates, minimizing the temperature lag in drops (<0.2°C). But active fractions and concentrations of clay particles were not measured, complicating any estimation of their active fraction, and hence, the temperature shift between modes.

Cooper (1980, hereafter Co80) sampled active IN from the troposphere in winter in Wyoming; observing that their activity spectra differed by about 10°C between contact- and immersion-freezing modes (see PK97). Dust IN probably prevailed (Pratt et al. 2009a, 2010a; E10) (section 3a). Parsimoniously, it is proposed that $\Delta T_{\rm CIN,DM}$ = 10 K from the study by Co80. An onset for contact freezing of about −4°C (PP73) implies $\Delta T_{\rm onset,DM}$ = 6 K, given the onset temperature for condensation/immersion freezing introduced above (−10°C).

2) PRIMARY BIOLOGICAL GROUP OF IN (X = BIO)

With the biological-IN group, LY83 observed a temperature shift of 3 K for the fraction, by number, of drops frozen as a function of temperature, between immersion- and contact-freezing modes of ice-nucleating bacteria. This was for temperatures at which most drops were frozen. The shift becomes about 1 K for the onset of freezing. Cooling was very slow, minimizing any temperature lag (<0.01 K). However, as with PP73, the aerosol particles were not counted. If numbers of bacteria on the surface of, and inside, each drop were comparable, then this would suggest $\Delta T_{\rm CIN,BIO}$ = 3° and $\Delta T_{\rm onset,BIO}$ = 1°C.

3) BLACK CARBON GROUP OF IN (X = BC)

Scarcely any reliable observations are available for the shift of black carbon between modes. So the same temperature shift as before is assumed ($\Delta T_{\mathrm{CIN,BC}} = 4.5$ K), introducing $\Delta T_{\mathrm{onset,BC}} = 4.5$ K.

4) MODIFICATION OF EP

The new parameters are listed in Table 1 (see also appendix A).

e. Requirement for black-carbon IN to have an intrinsically hydrophilic surface without much organic coating

The original EP assumed that all types of black carbon have equal propensity for ice nucleation. That assumption is changed for the following reasons.

Field and laboratory observations show that, whereas many of the fresh biomass-burning plumes from various vegetation types have active IN at temperatures as warm as −30°C (e.g., Petters et al. 2009a; Twohy et al. 2010; Pratt et al. 2011; section 3a), fresh urban fossil-fuel pollution tends not to nucleate much ice (K09). Black carbon may be a major ice-nucleating species in biomass-burning plumes (sections 3a and 4). If so, atmospheric black carbon in nature varies greatly in ice-nucleating ability according to the source. The aim is to treat such variability with the modified EP.

Biomass-burning differs from fossil-fuel combustion in many ways: 1) the temperature of combustion, which governs gas-to-particle conversion, soot's morphology and crystallographic structure, and rates of chemical reactions; 2) oxygen availability (air–fuel ratio) promoting volatile organics internally mixed with the black carbon and inhibiting its agglomeration; and 3) the variety of inorganic compounds, which can react to alter the black-carbon surface, with fuel type affecting chemical compositions of particles (e.g., Petters et al. 2009a; Adachi et al. 2010). Variability of such factors must be less in combustion engines, by design, than in biomass flames. So, optimum conditions for some proportion of black carbon to be ice-nucleating seem more likely to occur somewhere in biomass-burning flames.

Factors controlling black carbon's ice nucleation are discussed in appendix C. One such factor is the surface polarity of black carbon P_s. This is the number of water monolayers adsorbed onto it at 50% relative humidity (Popovicheva et al. 2008a,b) after all soluble material has been washed away. The quantity P_s is a measure of the intrinsic hydrophilicity of soot. Greater availability of oxygen in parts of the biomass-burning flames and more variety of inorganic compounds, relative to fresh fossil-fuel combustion, would promote P_s and, hence, ice-nucleating ability. The average fraction of surface area of each black carbon particle covered by, and in contact with, an insoluble organic coating is defined as F_{OC}. Such nonbiological organic coatings tend to inhibit ice nucleation F_{OC}. Biomass-burning particles likely have less of such coatings.

1) MODIFICATION OF EP FOR SUBZERO TEMPERATURES WARMER THAN −40°C

Contributions to the apparent contrast in ice-nucleating ability of black carbon between biomass-burning plumes and freshly emitted fossil-fuel pollution may arise from P_s, F_{OC}, and morphological–crystallographic properties. The last factor is poorly understood. Thus, the above observations, assumed to apply also at warm temperatures, are encapsulated by redefining $\alpha_{\mathrm{BC}} = \tilde{\alpha}_{\mathrm{BC}}\Xi$, where $\tilde{\alpha}_{\mathrm{BC}} = (1/3) - 0.03$ and

$$\Xi = \delta_0^1(P_s, P_{s,0}, P_{s,1}) \times \delta_1^0(F_{\mathrm{OC}}, F_{\mathrm{OC},0}, F_{\mathrm{OC},1}). \quad (6)$$

Black carbon in fresh urban fossil-fuel pollution is assumed to be intrinsically hydrophobic, so that $\Xi \approx 0$. This is due to either $P_s \le P_{s,0}$ or $F_{\mathrm{OC}} \ge F_{\mathrm{OC},1}$ (appendix C). For intrinsically hydrophilic black carbon in ice-nucleating biomass-burning plumes, it is assumed that $\Xi \approx 1$ because of $P_s > P_{s,1}$ and $F_{\mathrm{OC}} \le F_{\mathrm{OC},0}$. Between both extremes, $0 < \Xi < 1$ and Ξ increases with P_s and $1 - F_{\mathrm{OC}}$. Thermal soot and thermal oxidized soot with little and appreciable ice-nucleating abilities have P_s values of 1 and 2 monolayers, respectively (K09). This suggests $P_{s,0} \approx 1$ and $P_{s,1} \approx 2$. Values of $F_{\mathrm{OC},0}$ and $F_{\mathrm{OC},1}$ are uncertain. Parsimoniously, it is assumed that $F_{\mathrm{OC},0} \approx 0.1$ and $F_{\mathrm{OC},1} \approx 1$. The new parameters are in Table 1 (appendix A).

2) MODIFICATION OF EP FOR SUBZERO TEMPERATURES COLDER THAN −40°C

The above modification, $\alpha_{\mathrm{BC}} = \tilde{\alpha}_{\mathrm{BC}}\Xi$, is applied also at cold temperatures. Moreover, Ph08 defined a threshold saturation ratio with respect to ice, $S_{i,0}^{\mathrm{BC}}$, for the onset of heterogeneous ice nucleation at cold temperatures (T in degrees Celsius). It is used to evaluate H_{BC} (appendix A). From observations by C11 of insoluble organic coatings inhibiting soot's ice nucleation, we infer that $F_{\mathrm{OC}} \approx 0$ at 5% organic content and $F_{\mathrm{OC}} \approx 1$ for the 30% and 70% contents. So, $S_{i,0}^{\mathrm{BC}}$ is redefined as

$$S_{i,0}^{\mathrm{BC}} = \tilde{S}_{i,0}^{\mathrm{BC}} + \delta_0^1(F_{\mathrm{OC}}, F_{\mathrm{OC},0}, F_{\mathrm{OC},1}) \times \left[1.2 \times S_i^w(T) - \tilde{S}_{i,0}^{\mathrm{BC}}\right]. \quad (7)$$

Now $\tilde{S}_{i,0}^{\mathrm{BC}} = 1.3$, intermediate between humidities for the onset observed by DeMott et al. (1999, hereafter

D99)/K09 ($S_i \approx 1.4$) and by C11 ($S_i \approx 1.2$). The above values of $F_{OC,0}$ and $F_{OC,1}$ noted for warmer temperatures are applied. In reality, soluble coatings on atmospheric black carbon would initiate homogeneous aerosol freezing at $S_i < S_i^w$, as seen by C11. These are the conditions under which any soluble particle would freeze homogeneously. Homogeneous freezing is not treated by the EP.

Finally, soot from burning propane was observed to nucleate ice at temperatures as warm as −45°C for low humidities below water saturation by C11. There the original EP had predicted no ice nucleation. Hence, the range of temperatures for onset of ice nucleation [Ph08, their Eqs. (11)–(12)] during supercooling at humidities well below water saturation is broadened to $\Delta T^{BC} =$ 10°C for black carbon, replacing $\Delta T = 5$ K previously. The transition for soot during supercooling at very subsaturated humidities now occurs from −40° to −50°C (instead of from −45°C previously). For dust and PBAPs, $\Delta T^X = 5$°C remains unchanged. This is all summarized in Table 1 (see appendix A).

f. *Soluble organics that become glassy at extremely cold temperatures*

The original EP assumed that only insoluble species of aerosol can nucleate ice. That assumption is changed as follows.

Soluble organics have been observed to nucleate ice heterogeneously after becoming glassy at extremely cold temperatures. Mu10 observed this for citric acid aerosols (modal diameter of 150 nm) with a glass temperature of about 210 K. It was assumed that citric acid was representative of soluble organics in general. Active fractions observed by Mu10 (~0.1%) were consistent with those seen in field observations of subvisible cirrus at temperatures colder than 200 K near the subtropical tropopause by Froyd et al. (2010, hereafter Fr10) (section 3d). Conversely, field observations by Cziczo et al. (2004) of anvil cirrus showed that organics are preferentially excluded from residual particles sampled from cloud ice relative to clear air, at temperatures mostly warmer than 200 K. Onset of glassiness at temperatures of about 200–210 K, depending on the organic species, may explain this contrast between the two sets of field measurements. Alternatively, differences in humidity and chemical composition of the organic species between both field campaigns might be a possible reason too.

A simplified treatment of the IN activity of soluble organics is proposed. Observations from INSPECT cannot be used, since temperatures inside the CFDC were always warmer than about −65°C. Instead, observations of citric acid with the AIDA chamber (subscript "@") by Mu10 form the basis of the new treatment. Since active fractions observed by Mu10 were so small ($\ll$1%), $\mu_{solO} \ll 1$ and this new equation replaces Eqs. (1) and (2) for soluble organic IN:

$$n_{IN,solO} \approx \frac{H_{solO}(S_i, T) g_{glass} n_{IN,solO,@} \Omega_{solO}}{\Omega_{solO,@}}. \quad (8)$$

The fit to observed active fractions from Mu10 implies that $n_{IN,solO,@} = 10^6 \times (7.7211 S_i - 9.2688)/\rho_{@}$ kg^{-1}, for all $1.2 < S_i < S_i^w$. Outside this range, $n_{IN,solO,@}$ $(S_i < 1.2) = 0$ and $n_{IN,solO,@}(S_i > S_i^w) = n_{IN,solO,@}(S_i^w)$. Also, $\Omega_{solO,@} = 5.6 \times 10^{-5}$ m^2 kg^{-1} is the baseline surface area of organic aerosols (modal diameter of 150 nm) at AIDA observed by Mu10. As before, Ω_{solO} is the (ideal) total surface area of all soluble organic aerosols with diameters > 0.1 μm. Also, g_{glass} is the maximum fraction of aerosols that can become glassy and $\rho_{@}$ is the air density in the AIDA chamber near 200 K. As before, H_{solO} represents the onset of ice nucleation as either the supercooling or humidity below water saturation increase beyond certain thresholds:

$$H_{solO}(S_i, T) = \delta_1^0(T, -75°, -65°\text{C}) \times \delta_0^1(S_i, 1.2, 1.3). \quad (9)$$

New parameters (e.g., for ASDs) are summarized in Table 1 (appendix A). Finally, contact freezing is assumed not to arise from soluble organic IN. Cloud droplets cannot be supercooled to temperatures colder than about −40°C in nature.

3. Comparison of revised scheme with observations

a. *Aircraft data from ICE-L*

The Ice in Clouds Experiment–Layer Clouds (ICE-L) occurred in autumn 2007 over Colorado and Wyoming (Field et al. 2012). It involved coincident airborne measurements of ASDs, chemical composition of aerosols and the concentrations of ice, active IN, and cloud condensation nuclei (CCN). Shallow mixed-phase wave clouds were observed. ICE-L is apt for testing schemes of heterogeneous ice nucleation.

The partially revised EP was compared by E10 (their Fig. 9) with aircraft data from ICE-L for only one day—namely, 18 November 2007 ("flight 4"). The period selected, 2245–2330 UTC, was without much carbonaceous aerosol and without homogeneously nucleated ice. E10 did this comparison only after correcting the EP's baseline surface area of dust (section 2b). For that day, the revised EP was found by E10 to have an error of less than about 20% compared to IN measurements with the CFDC from the observed wave cloud, for large observational samples. Observed IN concentrations were similar to ice concentrations measured with a 2D-C probe in the clouds.

Without altering the baseline surface area of dust, the EP's prediction shown by E10 would have been a factor of 4 too high. Other modifications to the EP in the present paper were not used by E10. Yet these would not have affected the results of E10 because their wave cloud was much colder than the onset temperature of freezing for dust (section 2a) and dust IN were far more prolific during flight 4 than other IN species (section 3a).

1) Specification of inputs to empirical parameterization

The new EP is compared with observations from flights 1, 3, 4 (as in E10), 6, and 12 of ICE-L on 7, 16, 18, and 29 November and 16 December 2007, respectively. Observations in, and near, shallow mixed-phase wave clouds between the −25° and −29°C levels (about 5–7-km altitude MSL) were made during selected periods of 1927–2050, 1738–1842, 1920–2342, 1831–1900, and 1808–1912 UTC, respectively for the five flights. Such temperatures are too warm for homogeneous freezing of liquid particles and too cold for ice multiplication by rime splintering. These periods were identified by Twohy et al. (2010) as being without contamination along the flight path by homogeneously nucleated ice falling from aloft. This was because the cloud-top temperature was too warm for homogeneous freezing. Thus, heterogeneous ice nucleation should dominate the clouds' ice initiation (e.g., Field et al. 2012).

For each period of ICE-L, size distributions of dust, black carbon, and PBAPs are inferred by combining measurements from these aircraft probes:

- the ultrahigh sensitivity aerosol spectrometer (UHSAS; Particle Metrics, Inc., Boulder, Colorado) for the total concentration of all aerosols with dry diameters exceeding 0.1 μm and less than 1 μm;
- single-particle soot photometer (SP2) (Schwarz et al. 2006; Baumgardner et al. 2008) for black carbon concentration; and
- the aircraft aerosol time-of-flight mass spectrometer (A-ATOFMS) (Pratt et al. 2009b) for chemical composition of residues of cloud particles selected by a counterflow virtual impactor (CVI) (Noone et al. 1988).

The CVI collects cloud droplets and ice crystals larger than 8 μm and evaporates away all water substance, sampling their residues. The A-ATOFMS measures composition of residues with vacuum aerodynamic diameters d_{va} of between about 70 and 1200 nm during the flight. It optically detects particles with two lasers, 6 cm apart, measuring their velocity, and hence, d_{va}. They are then ionized with another laser and the ions then enter the spectrometer.

Cloud glaciation was observed with the 2D-C optical probe (Particle Measuring Systems) measuring ice concentrations within clouds. Ice nucleation was observed with the CFDC that measured active IN concentrations outside clouds (Rogers et al. 2001; E10). For each period, the 2D-C data for ice particles larger than 60 μm is conditionally averaged over in-cloud parts of it with temperatures between −25° and −29°C and without any ice more than 500 m above the flight level. Aerosol data are conditionally averaged over out-of-cloud segments. These are defined by θ_e being within ±1.5°C from the mean of in-cloud θ_e values for the sampled wave cloud without homogeneous ice. Observed concentrations of black carbon particles larger than 0.1 μm ranged from 500 to 3000 L^{-1} among the five flights near the wave clouds. Concentrations of ice particles larger than 60 μm, measured by the 2D-C probe in those clouds, were between about 0.5 and 5 L^{-1}.

ASDs of dust, black carbon, and PBAPs were derived from ICE-L aircraft observations of clear air in four steps:

1) A fit with three lognormal modes to the total ASD (UHSAS) was performed at submicron dry diameters for each flight, averaged over clear air near the wave cloud (Fig. 1). The first and second modes were assumed to consist of diverse aerosol species, as detected by the A-ATOFMS (Pratt and Prather 2010). When UHSAS data were insufficient to resolve the third (largest) mode, a geometric mean diameter of 0.8 μm and relative dispersion of 1.9 were assumed following Ph08 for dust.
2) Particles in the dust–metallic category (X = DM) were assumed to populate all of the third mode of this preliminary fit to UHSAS data from step 1 in all five flights. This was because dust was observed by the A-ATOFMS in clear air during most flights (Table 2). No coarse mode of dust with a supermicron modal diameter was assumed, as Eidhammer et al. (2009) neglected it because of high altitude. This initial estimate for dust's ASD was refined by comparing its "particle number fraction," $g_{X,0.1\rightarrow1}$ for X = DM, with that observed by A-ATOFMS (Table 2). This fraction $g_{X,0.1\rightarrow1}$ is the number of particles in group X, relative to all particles, with dry diameters between 0.1 and 1 μm. With the three flights (1, 3, and 12) for which dust was identified by the A-ATOFMS, the value of $g_{DM,0.1\rightarrow1}$ calculated from the initial estimate was much too low. For them, the first two modes from step 1 were then assumed to consist partly of dust, applying the observed value of $g_{DM,0.1\rightarrow1}$. That assumption is consistent with observed ASDs in desert-dust layers extending to small sizes (McConnell et al. 2008). Eventual dust ASDs were consistent with both UHSAS and A-ATOFMS data.

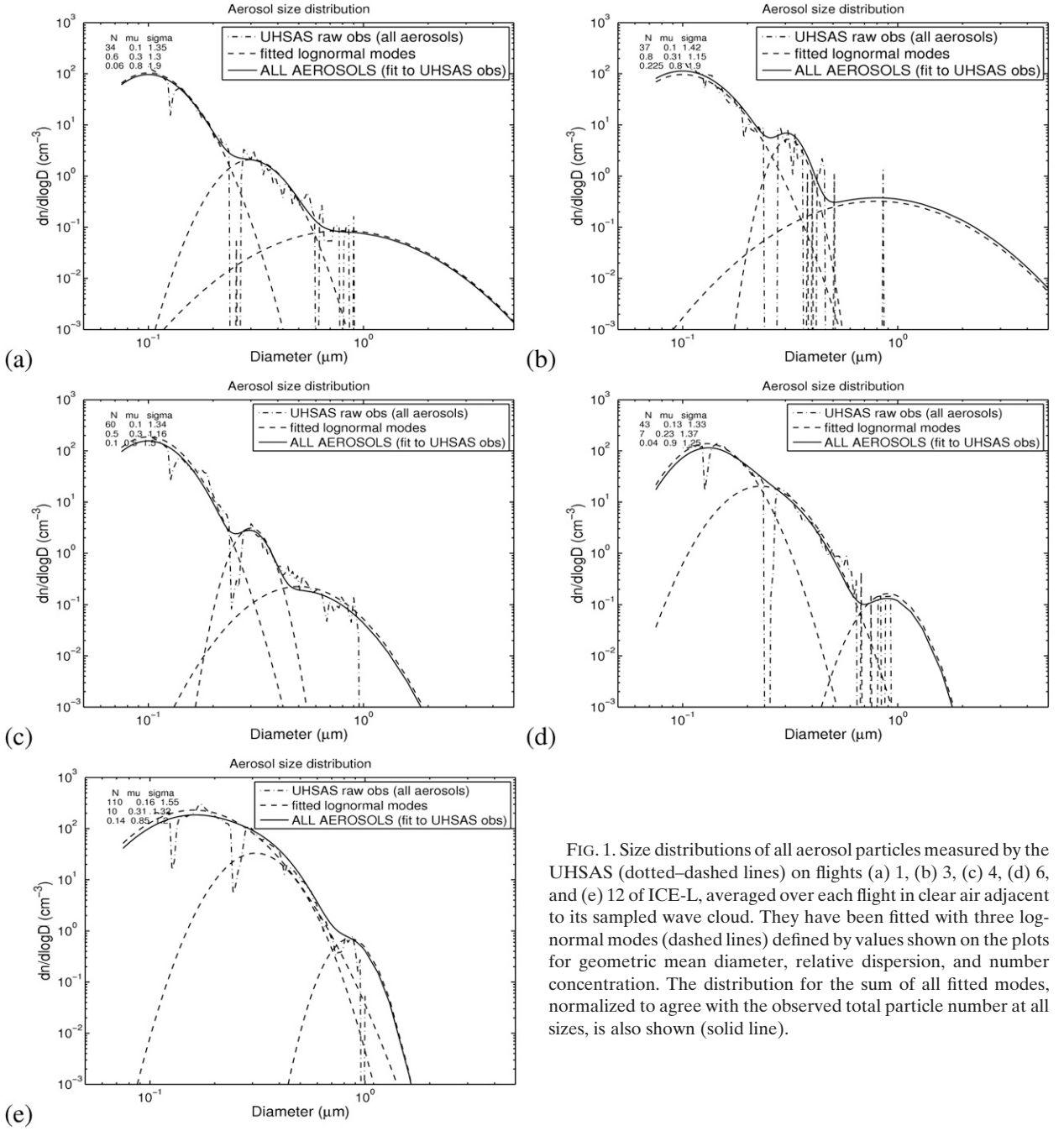

FIG. 1. Size distributions of all aerosol particles measured by the UHSAS (dotted–dashed lines) on flights (a) 1, (b) 3, (c) 4, (d) 6, and (e) 12 of ICE-L, averaged over each flight in clear air adjacent to its sampled wave cloud. They have been fitted with three lognormal modes (dashed lines) defined by values shown on the plots for geometric mean diameter, relative dispersion, and number concentration. The distribution for the sum of all fitted modes, normalized to agree with the observed total particle number at all sizes, is also shown (solid line).

3) PBAPs (X = BIO) were assumed to have an ASD with three lognormal modes having the same geometric mean diameters as those fitted to the UHSAS data. Their numbers of particles per mode were constrained by the observed value of $g_{\mathrm{BIO},0.1\rightarrow1}$ from the A-ATOFMS (Table 2). Standard deviation ratios were increased beyond values of the fitted modes (UHSAS) toward more realistic values observed by Matthias-Maser and Jaenicke (1995, hereafter M95) for similar modes of PBAPs (Table 1) as far as possible. This was done while ensuring that the combined size-distribution function of all PBAPs, dust, and soot was not significantly greater than that for all aerosols fitted in step 1. Bacterial, fungal, and viral material (M95), and their fragments, may have been among these PBAPs.
4) Black carbon (X = BC) was assumed to have a lognormal size distribution with the same geometric

TABLE 2. Observed aerosol conditions in clear air next to wave clouds for all periods, simulated by the EP, of flights in ICE-L. Number fractions for dust and PBAPs are the ratios of their number concentration for dry diameters between 0.1 and 1 μm, relative to the total concentration of all aerosols in that size range ($g_{DM,0.1\rightarrow1}$ and $g_{BIO,0.1\rightarrow1}$). These aerosol fractions were measured by real-time single-particle mass spectrometry (A-ATOFMS) on the flights; the sample size N_{MS} is shown for each flight. For some flights certain species listed were not detected (''n/d''). Shown is the SP2 data of total number concentration of black carbon particles N_{BC}. These data were combined with the observed total aerosol concentrations (UHSAS; Fig. 1) and used to constrain the eventual size distributions of insoluble aerosol, shown in Fig. 2, applied as inputs for EP simulations. Total number concentrations of dust and biological particles for all sizes (N_{BIO} and N_{DM}) from these eventual size distributions are also given.

ICE-L flight	N_{MS}	$g_{DM,0.1\rightarrow1}$	$g_{BIO,0.1\rightarrow1}$	N_{BC} (cm^{-3})	N_{BIO} (cm^{-3})	N_{DM} (cm^{-3})
1	33	15 (±6)%	12 (±6)%	0.8	4.2	5.2
3	40	5 (±3)%	<3% (n/d)	0.7	0	1.75
4	38	<3% (n/d)	3 (±3)%	0.5	1.8	0.1
6	60	<2% (n/d)	<2% (n/d)	1.7	0	0.04
12	198	1 (±1)%	<1% (n/d)	3.2	0	1.2

mean size as the smallest mode fitted to the UHSAS data from step 1. Its total number concentration was constrained by coincident SP2 measurements (Table 2). A standard deviation ratio (1.6) consistent with the size-resolved SP2 measurements of ICE-L, and following Ph08, was applied.

The ASDs of dust, black carbon, and PBAPs are shown in Fig. 2. Size-resolved SP2 and UHSAS data are also shown. These ASDs provided inputs of total surface area at all sizes > 0.1 μm to the EP for each flight. The size-resolved SP2 data, available only at dry diameters $<$ 0.2 μm, agree well with the fitted size distributions for black carbon in all flights (Fig. 2). Note that primary biological particles in ICE-L were only observed on two flights—namely, 1 (12% ± 6%) and 4 (3% ± 3%)—which is why they are evident in the ASDs only for both flights (Fig. 2). In summary, the ASDs for all five flights are based on ambient sampling in clear air around each cloud, which was without homogeneously nucleated ice and was simulated in the present paper.

Biomass-burning particles observed in ICE-L were aged by at least a few days, except for fresh plumes from prescribed burns. They had a high hygroscopicity from soluble coatings acquired (Pratt et al. 2010b). In flight 12 of ICE-L, almost all biomass-burning particles were seen to be internally mixed with sulfate (mass fraction ≈ 63%) mostly as sulphuric acid (hygroscopicity parameter: $\kappa \approx 1$), with organics [mass fraction ≈ 31%; $\kappa \sim 0.05$ (Petters et al. 2009b)], and with black carbon (mass fraction ≈ 2%) (Pratt et al. 2010b). Average hygroscopicity of soot-containing particles from biomass burning in ICE-L must have been $\kappa \approx 0.7$, so they were CCN-active at $s_w = 1\%$ for sizes greater than 0.1 μm (Petters and Kreidenweis 2007). That biomass-burning aerosols in ICE-L were both IN active (Twohy et al. 2010) and had high κ and low organic contents (<65%) is consistent with observations by Petters et al. (2009a) (section 2e). Biomass burning was the main source of black carbon in ICE-L, so $\Xi = 1$ is prescribed for the EP input.

Next the EP was run offline with the humidity prescribed at water saturation and an average in-cloud temperature and pressure (448, 453, 486, 558, and 595 mb, respectively, at flight level) from measurements in each of the five flights. The above ASDs of dust, black carbon, and PBAPs observed near each wave cloud, sampled close to this temperature, were applied as inputs. This average temperature was the geometric mean of temperatures at flight level (−28°, −25°, −27°, −26°, and −25°C, respectively) and cloud top (3°C colder). It approximated the coldest in-cloud temperature of parcels before sampling. Soluble organic IN were neglected because of this temperature. Contact freezing is predicted to be less prolific than other modes of IN activity in mesoscale systems consisting both of convective and stratiform clouds, whether outside in (Phillips et al. 2007) or inside out. Our recent analysis of simulations of mesoscale cloud systems by Phillips et al. (2009) supports this, as inside-out contact freezing was treated. Hence, all contact freezing is neglected for the present comparison. The justification for prescribing humidity in this way, instead of using a cloud model, is that the ascending regions of each simulated wave cloud of ICE-L were mostly mixed phase, where its ice and droplets were initiated (Twohy et al. 2010; E10). In mixed-phase cloud, the humidity is maintained close to water saturation by the liquid phase (Korolev and Mazin 2003; Korolev 2007). Little precipitation fell from above the flight level, and no known processes of ice initiation other than IN activation occurred. As argued by Ph08, at humidities close to water saturation the value of s_w should not affect ice nucleation in the cloud. All IN particles (>0.1 μm) should be immersed in cloud droplets anyway. So, it was unnecessary to model all of the cloud microphysics.

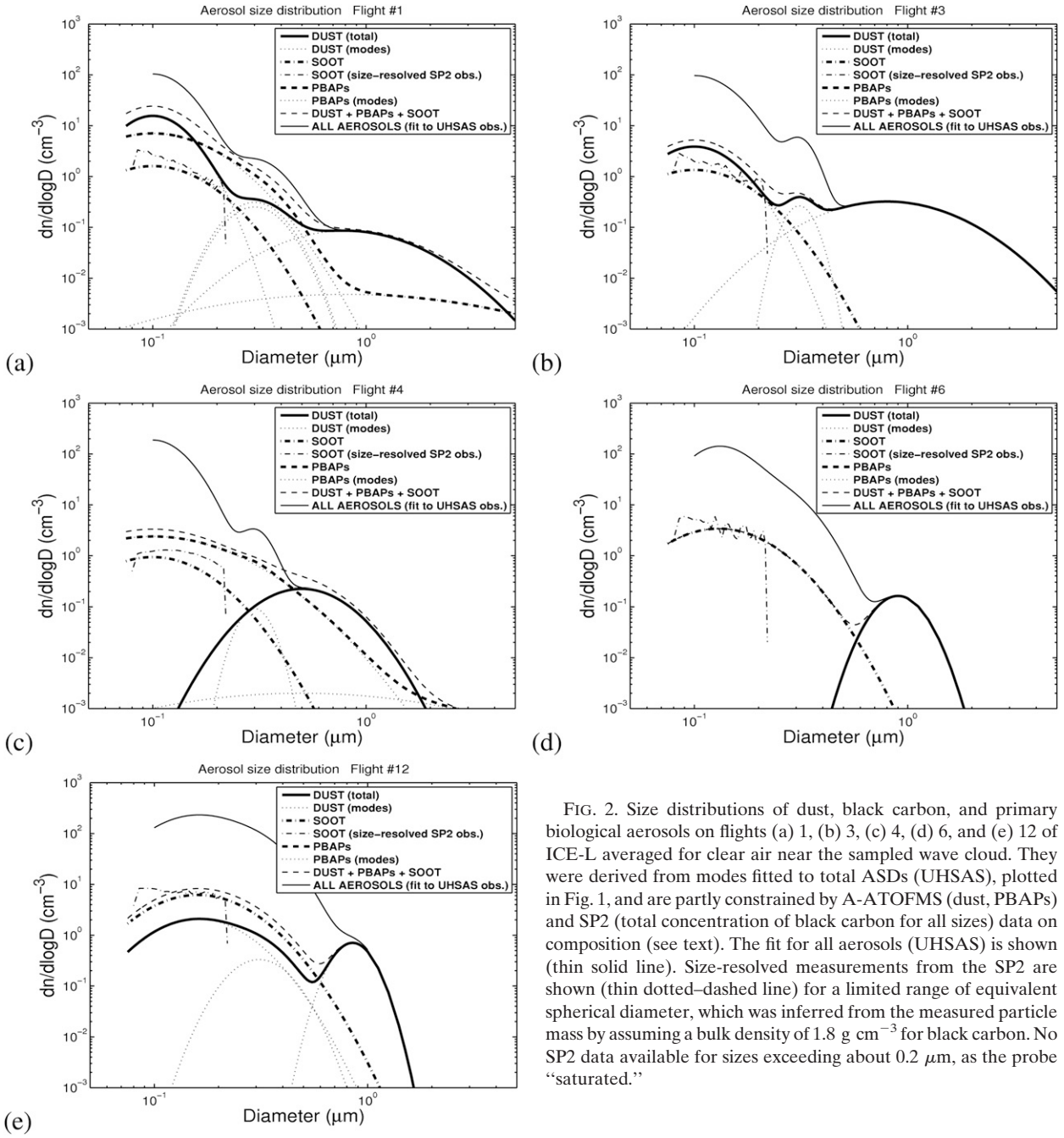

FIG. 2. Size distributions of dust, black carbon, and primary biological aerosols on flights (a) 1, (b) 3, (c) 4, (d) 6, and (e) 12 of ICE-L averaged for clear air near the sampled wave cloud. They were derived from modes fitted to total ASDs (UHSAS), plotted in Fig. 1, and are partly constrained by A-ATOFMS (dust, PBAPs) and SP2 (total concentration of black carbon for all sizes) data on composition (see text). The fit for all aerosols (UHSAS) is shown (thin solid line). Size-resolved measurements from the SP2 are shown (thin dotted–dashed line) for a limited range of equivalent spherical diameter, which was inferred from the measured particle mass by assuming a bulk density of 1.8 g cm^{-3} for black carbon. No SP2 data available for sizes exceeding about 0.2 μm, as the probe ''saturated.''

2) PREDICTIONS BY EMPIRICAL PARAMETERIZATION FOR FIVE ICE-L FLIGHTS

Figure 3a compares predictions by the revised EP (section 2) with observations of heterogeneously nucleated ice during the selected periods of five flights through mixed-phase wave clouds. Some flights (e.g., 6, 12) encountered carbonaceous aerosol from biomass burning. The predicted concentration of active IN at the temperature and humidity of the wave cloud has the same order of magnitude as the observed means of (i) active IN concentration from the CFDC outside clouds and (ii) ice (>60 μm) concentrations from the 2D-C probe within cloud. Averaging was done along the in-cloud traverse, selected with the above criteria. The 2D-C probe had been upgraded to have faster electronics, and reliably measured concentrations of ice crystals of sizes between 60 μm and almost 1 mm. Optical probes

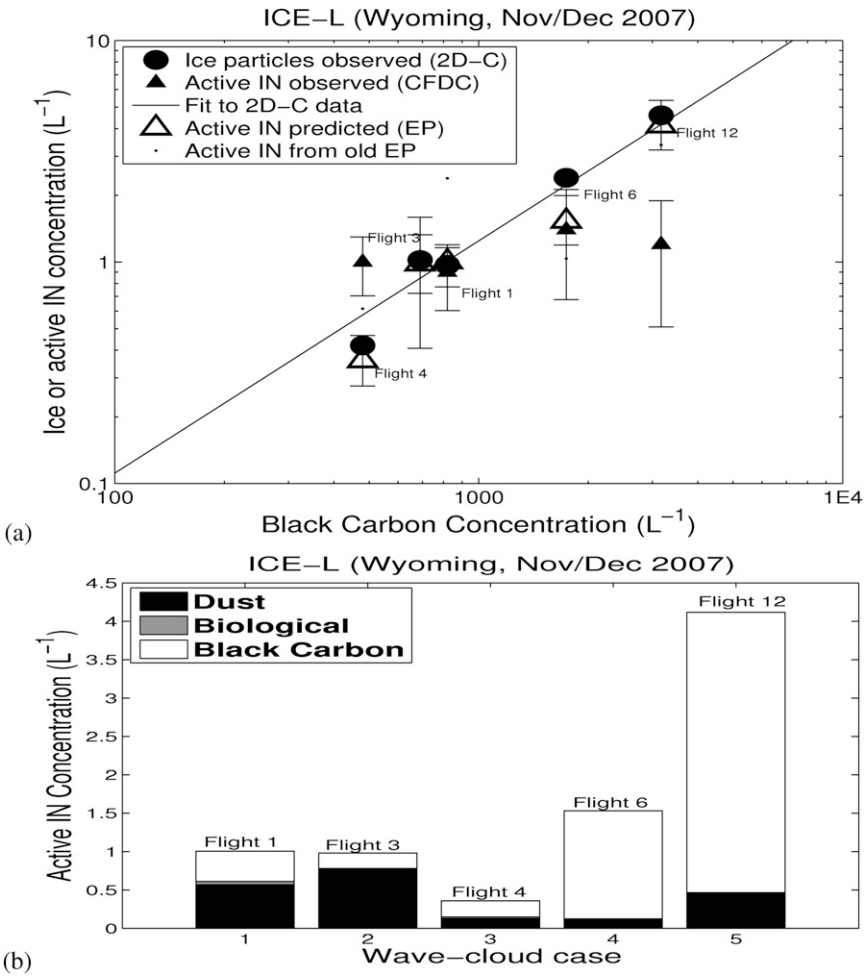

FIG. 3. (a) Comparison of the new EP's predicted IN activity (open triangles) for wave clouds (about −25° to −30°C, water saturation) observed by aircraft over Wyoming (ICE-L; Field et al. 2012) in flights affected to varying degrees by carbonaceous aerosol in plumes from biomass burning. The EP was run offline for observed ASDs of black carbon, dust, and insoluble organics inferred from aircraft data near each wave cloud sampled. Measured concentrations of IN from the CFDC (filled triangles) and ice (>60 μm; filled circles–solid line, right) from the 2D-C probe are plotted. Vertical lines (thin) on CFDC data are 90% confidence intervals of the mean IN concentration. Vertical lines (thin) on the EP predictions show uncertainty due to estimating coldest in-cloud temperatures of parcels before sampling by using temperatures at flight level and cloud top (base and top of error bars) instead of their geometric mean (open triangles). The EP differs by less than 50% from observed (2D-C) ice concentrations. The prediction from the old original version of the EP of Ph08 is shown (tiny dots). Also displayed is (b) the new EP's predicted composition of active IN for each flight plotted in (a).

flown on aircraft are prone to a high bias of the measured ice concentration due to shattering of ice on impact. Yet this tends to be less important when ice particles are all smaller than 0.6 mm (Korolev and Isaac 2005), as seen in the simulated periods of ICE-L wave clouds. The approach is taken, following Field et al. (2012), that the ICE-L wave clouds may be assumed to be ''natural IN counters.'' Nucleated ice merely follows the flow through each cloud. So, their ice concentrations measured with the 2D-C probe are assumed to be a measure of active IN concentrations. In view of the uncertainty in the prediction from estimation of the coldest in-cloud temperature in parcels before sampling (error bars of open triangles on Fig. 3a) and from specifying ASDs of each species, the EP is consistent with the 2D-C data. Relative to observed 2D-C concentrations [(ii) above], the EP's

prediction has an error of less than about 50% for each of the five flights.

A trend of proportionality between concentrations of heterogeneously nucleated ice (2D-C) and black carbon (SP2) was observed by Twohy et al. (2010) for the same periods of these five flights. This observed trend is reproduced by the revised EP (Fig. 3a, open triangles and full line). The EP predicted the trend in terms of IN activity only of black carbon (Fig. 3b). PBAP IN and dust IN, as parameterized, do not explain it. For two of the flights (6 and 12), black carbon is predicted to comprise most of the active IN. Most black carbon (soot–elemental, as observed by A-ATOFMS) was internally mixed with inorganic salts (e.g., SO_4, NO_3, K, NH_4) and organics in biomass-burning particles on those days. (The original version of the EP from Ph08 predicted a much weaker trend than was observed owing to different baseline surface areas causing more activity of dust IN and less for soot IN, relative to the new version).

The trend of IN versus black carbon concentration, due primarily to flights 6 and 12, is not evident in the CFDC measurements. The CFDC needs a low (1 L min^{-1}) flow rate so as to expose IN to steady conditions for several seconds. This causes a larger sampling uncertainty for estimates of mean IN concentrations (see error bars on Fig. 3a), even for the sample periods (up to several min) spent in clear air feeding into clouds when IN number concentrations are low.

Figure 3b also shows that for flights 1 and 4, PBAPs are predicted by the EP to contribute 0.02 and 0.04 L^{-1} (about 5%), respectively, to overall concentrations of active IN. This prediction is uncertain since no direct measurements of supermicron PBAPs or of IN-specific compositions were attempted during ICE-L. Dust IN was predicted to be more prolific than biological IN by about one order of magnitude on both flights.

In aircraft observations of ice-only parts of simulated periods (no homogeneous ice), the A-ATOFMS measured this chemistry of cloud-ice residues: 1) salt (NaCl, 5% ± 22%), organic carbon/nitrate (40% ± 17%), black carbon (5% ± 2%), primary biological (20% ± 20%), and dust (30% ± 19%) in flight 1; and 2) salt (Na–K–Ca–Mg–Cl, 42% ± 10%), salt dust (Na–K–Ca–Mg–Cl silicates, 54% ± 10%), and black carbon (4% ± 4%) in flight 3. The ice residues consisting of organic–nitrate mixtures and salt (NaCl, Na–K–Ca–Mg–Cl) are unlikely to have acted as IN (Cziczo et al. 2004; Pratt et al. 2009a, 2010a). However, because of the possibilities of ice having scavenged aerosol material, and possible splash–shatter artifacts and breakup of large ice particles within the CVI, it is not certain that the cloud-ice residues classified as black carbon, biological, and dust had acted as IN. Moreover, there is the chance of creation of multiple aerosol particles during freezing of each cloud-droplet in cloud (e.g., when solute becomes solid) or during evaporation in the CVI. Qualitatively, the cloud-ice residues were mostly enriched in the same species predicted to have acted as IN by the EP on both flights (Fig. 3b), relative to aerosol particles sampled from clear air.

Four flights (1, 3, 4, and 12) were analyzed by Pratt et al. (2009a, 2010a,b) and E10. Residues were sampled when homogeneous ice was present, outside the time periods identified by Twohy et al. (2010) and simulated by the EP. There was enrichment of cloud-ice residues seen in (i) mineral dust and PBAPs (soot was present in cloud-ice residues though not enriched) in flight 1 (Pratt et al. 2009a); (ii) dustlike playa salts containing silicates from dry salt playas in flight 3 (Pratt et al. 2010a), as suggested also by E10 for flight 4 (e.g., Koehler et al. 2007); and (iii) black carbon during flight 12 (Pratt et al. 2010b). Pratt et al. (2009a, 2010a,b) and E10 hypothesized that these may have been the dominant species of active IN. Qualitatively, the EP predicts that these same species of IN [(i)–(iii)] governed the heterogeneous ice nucleation in each flight (1, 3, 4, and 12) (Fig. 3b). No quantitative validation of the EP's prediction of IN composition is possible, however, because IN composition was never measured directly during ICE-L.

b. Laboratory observations of ice nucleation by dust, soot, and PBAPs

Figure 4a shows laboratory measurements published in the literature for surrogate dust material (plotted in red or orange), in comparison with field observations (in blue or turquoise). It shows the number of active IN per unit surface area of dust particles (ζ) in the range of sizes that could activate in the CFDC (0.1–1 μm) at the time of these observations and at humidities below water saturation. Although a similar plot was displayed by Ph08, it is extended here by including recent laboratory data (F06; Möhler et al. 2006, 2008; Koehler et al. 2010, hereafter K10; D11; N12).

At temperatures colder than about −40°C, ζ of relatively fresh dust in the laboratory is mostly about two orders of magnitude higher than average values from CFDC field observations of natural atmospheric dust from the background troposphere (INSPECT). This laboratory data are for surrogate aerosol material (e.g., collected from the ground) observed in the AIDA chamber (F06; Möhler et al. 2006) and by Archuleta et al. (2005). The contrast occurs despite the humidity imposed inside the CFDC being slightly higher (Fig. 4b). Arguably, some of the difference could be due to association of the laboratory data with particles that are solely dust, while atmospheric values are for dilute conditions for which the dust contribution must be inferred.

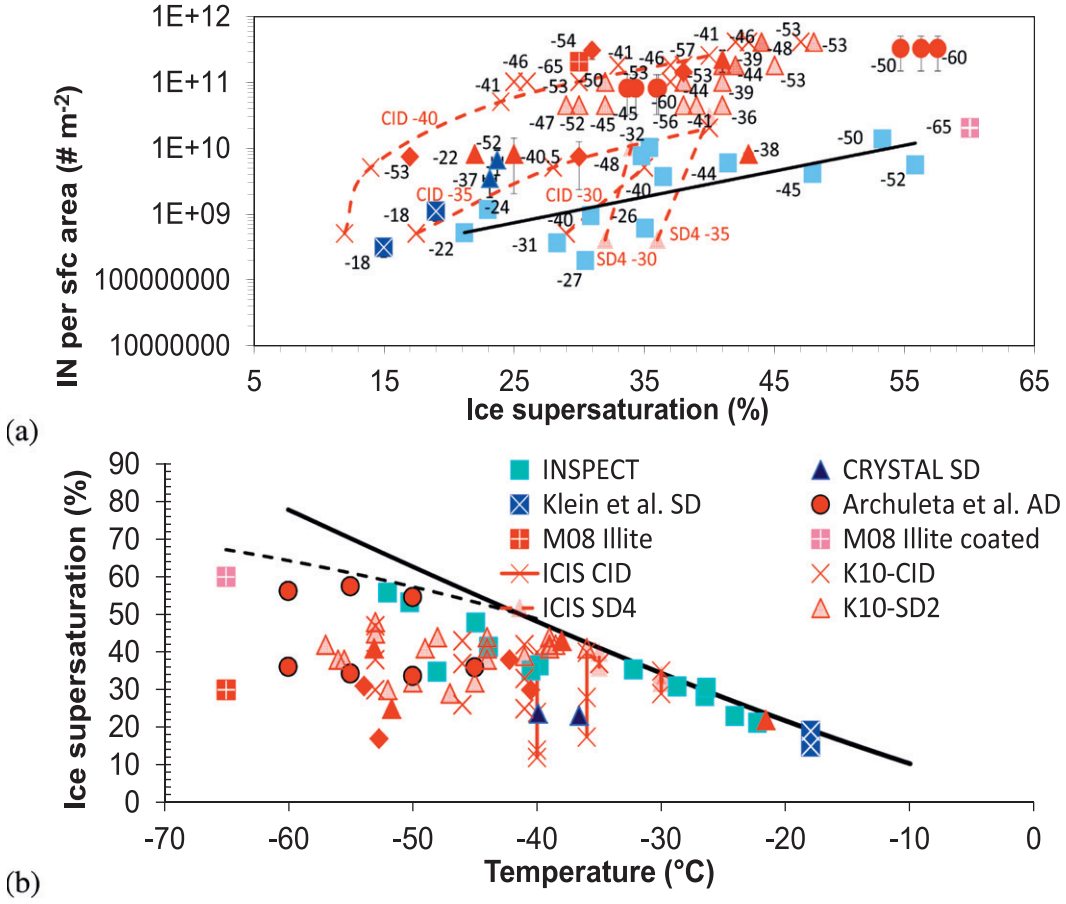

FIG. 4. (a) The ratio ζ of measured IN number to surface area [No. m^{-2} (dust)] of dust particles with diameters $<$ 1 μm as a function of supersaturation with respect to ice (s_i) at humidities well below water saturation and (b) conditions of temperature and s_i for the same measurements. Field observations of atmospheric aerosol (blue or turquoise) are compared with laboratory observations of surrogate aerosol material (red or orange). Field observations are from INSPECT-1 and -2 (Colorado) with the CFDC (DeMott et al. 2003a; Richardson et al. 2007), for the background troposphere (light blue or turquoise squares), and for freshly emitted dust from the Sahara in CRYSTAL-FACE with the CFDC (near Florida; DeMott et al. 2003b) (dark blue triangles), and from Kleiner Feldberg in Germany (Klein et al. 2010) (dark blue squares). Laboratory observations are from Archuleta et al. (2005) (filled red circles) and AIDA (F06; Möhler et al. 2006) for Saharan (SD) and Asian (AD) soil dust from the ground (red triangles and diamonds, respectively) for first and subsequent expansions (open and filled). Illite was observed (AIDA) at -65°C before and after coating with soluble material (Möhler et al. 2008) (filled red squares, dark and light, respectively), suppressing IN activity. CFDC observations for ice nucleation below water saturation by soil dust from the Sahara (e.g., SD4) and Canary Islands (CID) are shown (dashed red lines with red crosses, red hatched triangles and circles) (D11; K10). Temperatures (numbers, °C) are labeled in (a). The original plot was by Ph08 (their Fig. 1).

However, ζ is much higher also for freshly emitted atmospheric dust observed with the CFDC, in the Cirrus Regional Study of Tropical Anvils and Cirrus Layers–Florida-Area Cirrus Experiment (CRYSTAL-FACE) in July 2002 (DeMott et al. 2003b), relative to INSPECT, as noted by Ph08. It is conceivable that kinetic limitations of vapor growth of ice to detectable sizes at temperatures colder than -40°C might have limited the assessment of IN concentrations during INSPECT. Richardson et al. (2010) found that kinetic factors limited detection of the onset relative humidity for homogeneous freezing for the version of the CFDC deployed in INSPECT. It is not presently clear if such measurement issues can explain the entire difference in ζ by two orders of magnitude, but it appears unlikely.

At temperatures warmer than about -35°C, there is uncertainty about the general applicability of this result about higher nucleating ability of surrogate aerosol material than atmospheric aerosols. Some data for surrogate dust from the ground (K10; D11) in the Sahara and Canary Islands show ζ values similar to atmospheric dust (INSPECT) (Fig. 4a). Fresh atmospheric dust observed

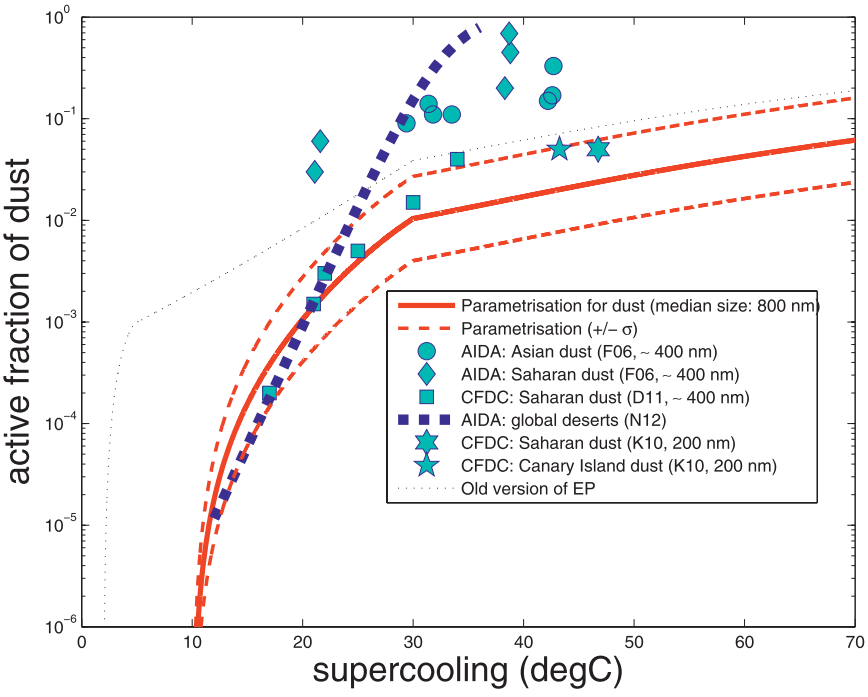

FIG. 5. Comparison of the frozen fraction of dust predicted by the parameterization with laboratory results from the AIDA chamber for immersion and condensation freezing from F06. The AIDA data are filtered to be close to water saturation ($S_i > S_i^w - 0.15$, where S_i^w is the saturation ratio with respect to ice at water-saturated conditions). Error lines are displayed for the scheme's prediction, based on uncertainties (relative errors) in its parameters, using a statistical model as clarified by Ph08. Also shown is laboratory data (CFDC) for Saharan soil dust from D11 and K10, who also observed Canary Island dust. The fit, for ice number ($\propto$ surface area) by N12, to AIDA observations of dust from Israeli, Saharan, and Asian deserts is shown. This fit is applied to the same size distribution assumed for the EP. The original version of the EP from Ph08 is also plotted (thin dotted line).

in Germany at −18°C (Klein et al. 2010) has a similar value of ζ to INSPECT.

The hypothesis of microphysical and possibly chemical processing of natural atmospheric dust acting to lower its nucleating activity during long-range transport (Ph08) is still consistent with our analysis of most laboratory and field-campaign data, at least at the colder subzero temperatures. Consistent with such a role for atmospheric processing, when illite particles at −65°C are coated with soluble material (Möhler et al. 2008), their value of ζ is in good agreement with the CFDC observations of atmospheric aerosol (INSPECT). It was two orders of magnitude higher without the coating (Fig. 4). Such impacts from soluble coatings were not seen for freezing at temperatures warmer than −40°C by Sullivan et al. (2010a), though they may strongly affect deposition nucleation. Thus, soluble coatings on the soot-containing (e.g., biomass-burning) or silicate-containing particles in ICE-L cases would not be expected to have influenced directly the ice nucleation observed in the mixed-phase wave clouds near −28°C and water saturation. This justifies our lack of explicit treatment of such soluble coatings in the EP above.

Comparison of the new version of the EP with some of this laboratory data, not used in its construction, is shown in Figs. 5 and 6, for condensation/immersion freezing by dust and black carbon. The EP is run offline with humidity prescribed at water saturation, as before. Similar plots were shown by Ph08, but are reproduced here with the recent laboratory data. Parameter values of ASDs for the prediction are as assumed by Ph08 for the background troposphere, except for changes in Table 1. The ASD parameters include, for dust, black carbon and PBAPs, geometric mean diameters of 0.8 (3.0), 0.09, and 0.163 (0.466) μm and standard deviation ratios of 1.9 (1.6), 1.6, and 2.54 (3.96), respectively, for each first (second) lognormal mode. For dust and PBAPs, ASDs are bimodal with ratios of total numbers in each mode of 150:1 and 347:1, respectively. For the comparison, soot in the background troposphere is assumed to be intrinsically hydrophilic because of chemical processing, so $\Xi = 1$ (section 2e). Homogeneous freezing is

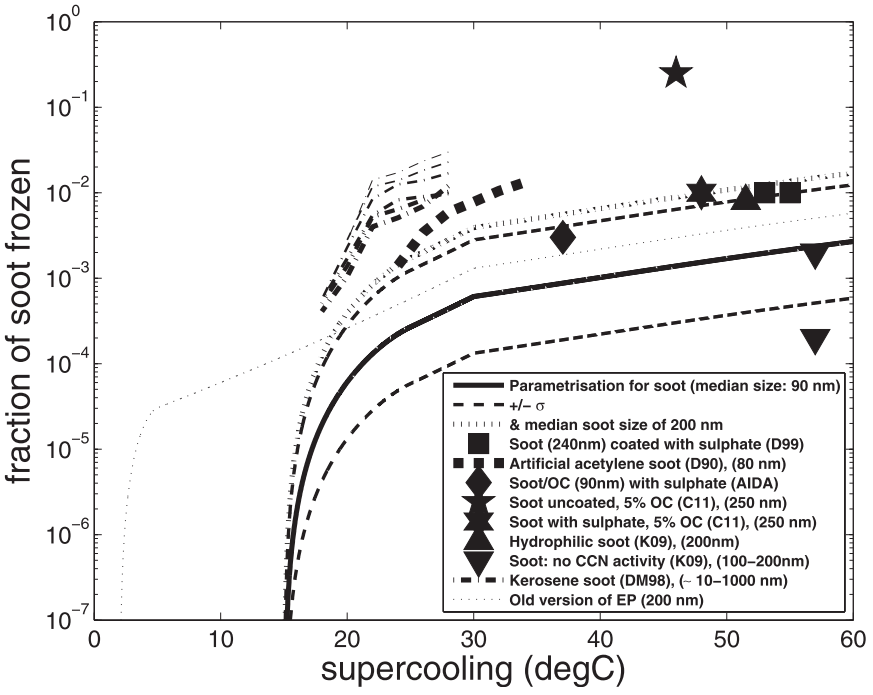

FIG. 6. Fraction of black carbon that is frozen, predicted by the new version of the EP (solid line) and observed in laboratory studies of surrogate samples of black carbon by D90, D99, Möhler et al. (2005a; AIDA), K09, and C11 (filled symbols). The D90, D99, AIDA, and C11 observations concern black carbon from combustion of acetylene, lamp black, sparking of graphite electrodes, and burning propane, respectively. The surrogate black carbon was coated with sulfate (except for one data point of C11). The K09 observations concern black carbon with little CCN activity (termed ''TC1'' and ''thermal soot'' by K09; denoted by ''hydrophobic'' on the plot) from combustion of kerosene and natural gas, and hydrophilic black carbon with much CCN activity (termed ''thermal oxidized soot'' by K09; labeled as ''hydrophilic'' on the plot) created by immersing such hydrophobic black carbon in acid for a month. Assumed aerosol parameters for the EP's prediction are those estimated for the background troposphere (median black carbon diameter of 90 nm). Ice nucleation from K09 and D99 displayed here was at relative humidities (87% and 93% for D99) slightly below those required for homogeneous aerosol freezing. Also shown are active fractions of a broad size distribution of immersed submicron black carbon particles [~(10–1000) nm], inferred from fractions of drops frozen observed by DM98 (see section 2a) (dashed–dotted lines with thickness increasing over drop diameters of 0.34, 0.39, 0.46, 0.58, 0.69, and 0.80 mm). Errors are displayed for the scheme's prediction (parallel thin dashed lines), based on errors in its parameters, as clarified by Ph08. Also shown are a prediction by the new EP with a larger median size of black carbon (200 nm) (thicker dotted line) and the original version of the EP from Ph08 assuming this size (thinner dotted line).

excluded. The EP portrays IN activity of natural atmospheric aerosol while the laboratory observations are of surrogate aerosol (e.g., land surface collections). For this reason, and because of differences in mean sizes of ASDs, exact agreement is not expected.

For mineral dust (Fig. 5), there is good agreement of the freezing fraction of Saharan soil dust (geometric mean diameter of 0.4 μm, standard deviation ratio of 1.7) observed in the laboratory by D11 with the prediction at temperatures warmer than -30°C. The prediction is lower than the observations at colder temperatures, by an order of magnitude. If the geometric mean diameter of the EP input (0.8 μm) were adjusted to match the size of the soil dust (about 0.4 μm), the predicted active fraction would be further reduced by over half an order of magnitude. Any active fraction is almost proportional to the average surface area per particle. Similarly, the active fraction of the prediction at temperatures colder than -20°C is an order of magnitude lower than in AIDA observations of at least one other study of samples of surrogate dust from the ground in the Sahara and Asia (F06). It is seen despite this surrogate dust also having a mean size about half of that assumed for the EP's input.

At temperatures colder than about −25°C, active fractions of dusts collected from the ground in Israeli, Saharan, and Asian deserts (same ASD as the EP input) and observed in the AIDA chamber (N12) are up to two orders of magnitude higher than the prediction. Yet they agree well with EP at temperatures warmer than this. At temperatures colder than −40°C, the active fraction seen by K10) for Saharan and Canary Island soil dust (0.2 μm) agrees with the prediction. But the prediction would become an order of magnitude lower if dust particles were given the same size as observed in that study (0.2 μm). These discrepancies are not necessarily a problem because surrogate dust used in laboratory studies was shown by Ph08 (their Fig. 1) to have at least an order of magnitude more active IN per unit surface area than the natural atmospheric dust represented by the EP. That observed difference is shown above to be robust for new extensive laboratory data (Fig. 4a).

The active fraction for black carbon (Fig. 6, solid line) predicted for the background troposphere is lower by 50% than predicted previously by Ph08. This is mostly due to our revised value for the median diameter of black carbon (90 nm, about half of the previous size) in the background troposphere, with less surface area per particle.

The EP agrees well with observations at −52° to −55°C of hydrophilic (K09) and hygroscopic (D99; C11) black carbon with diameters of 200 nm if the prediction uses this as its assumed median size (Fig. 6, long thick dotted line). The predicted active fraction then differs from them by less than about 30%. Similarly, in the real troposphere, black carbon is usually observed to be internally mixed with soluble material, as in ICE-L (section 3a). The predicted active fraction for the standard size (90-nm diameter, thick solid line) of black carbon is 1) up to about one order of magnitude less than observed for hydrophilic black carbon of a similar size (80–90 nm) by D90 and Möhler et al. (2005a); 2) almost an order of magnitude higher than, or similar to, that observed for (e.g., hydrophobic) black carbon with little CCN activity by K09; and 3) much lower, by between one and two orders of magnitude, than that inferred (section 2a) from drop-freezing experiments by DM98, at about −20° to −28°C (modal black carbon size of 100–200 nm). The prediction is consistent with all of the observations in view of its uncertainty (see Ph08 for error analysis) and the differences between observations.

The predicted frozen fraction of PBAPs was compared with the same set of observations of bacterial IN used by Ph08 (e.g. Lindow et al. 1978; Gross et al. 1983; Hirano et al. 1985). It is intermediate between all of the observed fractions. The plot by Ph08 for the comparison is similar to that for the new EP, so is not shown again.

In summary, differences between the prediction for each IN species and laboratory data are less than, or comparable to, differences between these observations. Yet especially at colder temperatures, the prediction is lower, as expected for natural dust from Fig. 4.

c. *Field observations of ice nucleation by PBAPs*

Validation of the EP's treatment of biological ice nucleation is performed for a case of coincident observations of concentrations of both active PBAP IN and PBAPs from Colorado. At SPL during the first week of April 2008, a mass concentration of 0.61 μg m^{-3} for PBAPs with diameters > 0.5 μm is inferred from observations by Wiedinmyer et al. (2009, hereafter W09) (appendix B). The ASD of PBAPs is inferred from this observed mass concentration by assuming values of the mean size and standard deviation ratios of modes observed by M95 elsewhere. In the same week at SPL in April 2008, Bowers et al. (2009) measured an average concentration of 23 m^{-3} for active PBAP IN (bacteria, fungi, or pollen) at −10°C. The revised EP is run offline at water saturation using this ASD from observations at SPL. It predicts 30 m^{-3} of active PBAP IN at −10°C, which agrees with the observations. Bowers et al. (2009) observed that some of the bacteria in the ambient air belonged to families known to include ice-nucleating species.

d. *Field and laboratory observations of ice nucleation by soluble organics*

The new EP treats the IN activity of soluble organic aerosols (section 2f). Idealized runs of the EP at water saturation (section 3b) were performed with a soluble organic ASD using parameters in Table 1. Empirical knowledge is scarce for soluble organic IN. Figure 7 compares observed active fractions of soluble organic IN with those predicted by the EP at water saturation. There is good agreement of the prediction with field observations from just below the tropical tropopause in the Costa Rica Aura Validation Experiment (CR-AVE) during winter 2006 over the Pacific Ocean and South America by Fr10. Heterogeneous ice nucleation by organics was inferred by Fr10, as the maximum of S_i observed (1.35) in Cr-AVE precluded homogeneous freezing. Data for citric acid (Mu10) agrees well with the prediction, by design (Fig. 7). Ice was seen by Mu10 to be nucleated heterogeneously only at temperatures colder than the glass temperature at ice saturation T_g of 212 K. The threshold behavior observed by Mu10 is reproduced by the EP by design.

Laboratory data from Wilson et al. (2012, hereafter W12) for other soluble organic species are compared with the prediction in Fig. 7: 4-hydroxy-3-methoxy-DL-mandelic acid (HMMA; T_g = 237 K), raffinose (T_g = 241 K), levoglucosan (T_g = 212 K), and an internal mixture of raffinose with five dicarboxylic acids and

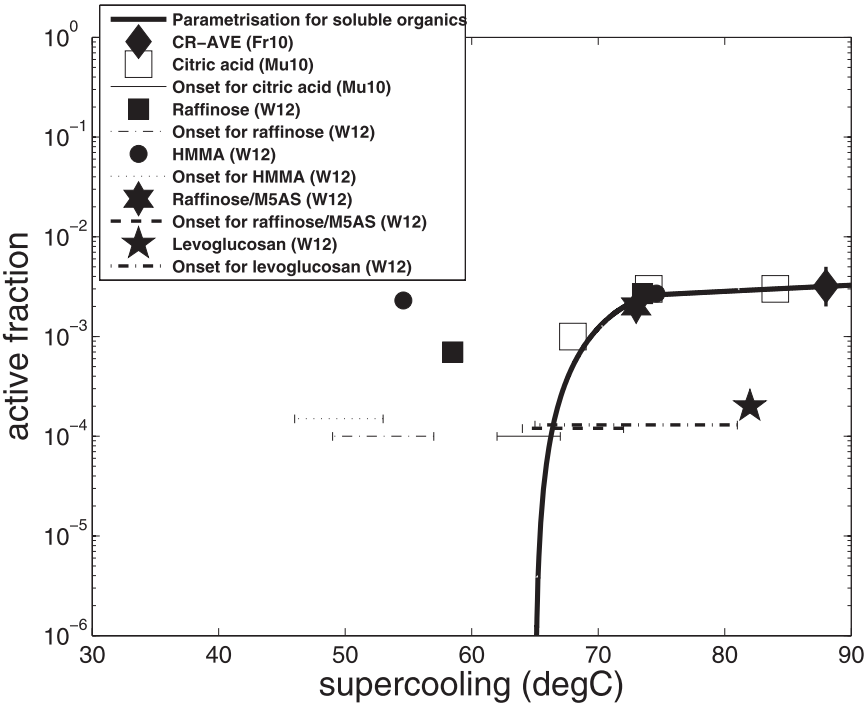

FIG. 7. Fraction of soluble organic aerosols that nucleated ice, predicted by the parameterization close to water saturation (solid line) and observed in subvisible cirrus near the tropopause in the subtropics over the Pacific and Americas from CR-AVE by Fr10 (filled diamond). Data (open square symbols) from Mu10 for citric acid agrees with the EP by design, as it was used in its construction. Similarly, for other soluble organic species, laboratory observations at AIDA (W12) are also shown (various filled symbols). These are 4-hydroxy-3-methoxy-DL-mandelic acid (HMMA), raffinose, levoglucosan, and a more representative internal mixture of raffinose with five dicarboxylic acids and ammonium sulfate ("raffinose–M5AS"). Data from W12 were not used in construction of the EP. For all laboratory observations displayed, the possible range of the onset temperature for detectable ice nucleation (an active fraction of about 1×10^{-4}) during supercooling near water saturation is inferred (various thin lines with bars). The experimental uncertainty was due to the limited numbers of experiments performed at AIDA.

ammonium sulfate ("raffinose–M5AS"; $T_g = 210$ K). The predicted active fraction is intermediate between these observations for each species. Moreover, the range of possible temperatures for onset of detectable heterogeneous ice nucleation, during supercooling at a humidity just below that for homogeneous aerosol freezing, is inferred from the published data. Each range for the onset is plotted on Fig. 7. The predicted onset near −65°C is consistent with that inferred for raffinose/M5AS and levoglucosan, in view of the experimental uncertainty. Raffinose–M5AS is supposed to be especially representative of soluble organics in the tropical upper troposphere (W12). The predicted onset is about 10–20 K colder than that inferred for HMMA and raffinose because of their warmer glass temperatures. For all species observed by W12, a threshold behavior with an onset near the glass temperature is seen. This behavior is qualitatively similar to that seen for citric acid and represented by the EP.

By contrast, Wagner et al. (2011) observed (AIDA) ice nucleation at −30°C by surrogate aerosols that were internal mixtures of salt (NaCl) with oxalic acid dihydrate (OAD). Solid crystalline OAD was supposed to nucleate the ice. Baustian et al. (2011) and Shilling et al. (2006) observed ice nucleation by solid crystalline particles of glutaric and maleic acid, at temperatures as warm as about −38° and −53°C, respectively. Such laboratory observations contrast with aircraft observations of cirrus in the troposphere at similar temperatures (Cziczo et al. 2004) (section 2f). So, they are not compared here with the EP. It is unclear whether such crystalline organic particles are prolific in the real troposphere. This is an area for future development of the EP.

4. Summary

Modifications to the empirical parameterization (EP) of ice nucleation have been developed in the present

TABLE 3. Summary of the new version of EP. Aerosol species and their modes of ice nucleation are listed, with the corresponding equations. Equations listed as ''unchanged'' are from the original version by Ph08, although they may include some parameters with new values given in the present paper (Table 1). Aerosol species are dust–metallic aerosols (X = DM), black carbon (X = BC), primary biological aerosol particles (X = BIO), and soluble organics (X = solO).

Aerosol species (X)	Ice nucleation mechanisms	New equations (section 2)	Unchanged equations	Conditions of T
(DM, BC, BIO)	Condensation/immersion freezing and deposition	Eqs. (4), (6), and (7)	Eqs. (1) and (2); Ph08 [their Eqs. (1)–(13)]	$T < (-10°, -15°, -2°)$C
	Contact freezing (inside out and outside in)	Eq. (5)	Ph08 [their Eqs. (15) and (16)]	$-37° < T < (-4°, -10.5°, -1°)$C
solO	Condensation/immersion freezing and deposition	Eqs. (8) and (9)	—	$T < -65$°C

paper. Baseline surface areas and temperatures for onset of freezing have been revised. A new group for PBAPs replaces the previous group of insoluble organic aerosols. The revised EP is sensitive to black carbon's properties. Aged biomass-burning particles, as seen in ICE-L, are assumed to have the potential to nucleate ice because they contain black carbon that has a hydrophilic surface, which is not encased by insoluble organic coatings. Soluble organics become a new fourth group of IN that is active at temperatures sufficiently cold for glassy states.

Details of how to implement the EP were noted by Ph08 and Phillips et al. (2009). The present modifications extend the range of its applicability to include the coldest temperatures found in the troposphere (e.g., −100°C) and more extreme conditions of aerosol chemistry. An overview of the new scheme is given by Table 3, showing the aerosol species, ice nucleation mechanisms, the key equations, and thermal conditions.

The prediction by the revised EP agrees with aircraft observations from five ICE-L flights of the IN activity and ice concentrations through wave clouds between −25° and about −30°C. This is found both for cases in which dust IN (e.g., E10) and black-carbon IN (section 3) prevail in overall ice nucleation. An observed trend between heterogeneous ice and black carbon concentrations noted by Twohy et al. (2010) among the five wave clouds in ICE-L is predicted by the revised EP to be due to heterogeneous ice nucleation by black carbon. The error in the prediction relative to ice concentrations observed in cloud by the 2D-C probe is less than about 50% for all five wave cloud cases from ICE-L. Such errors partly arise from inaccuracies of ASDs used for the EP's inputs, in view of the large sampling errors of A-ATOFMS measurements of single-particle composition in clear-air constraining them (Table 2).

The overall accuracy of the EP, when applied to ICE-L, is adequate for correct prediction of the order of magnitude of cloud-ice number concentrations in an atmospheric model. For warm clouds, errors of less than 50% in droplet concentration would cause a relative error of less than 10% both in cloud albedo and in the first indirect effect (see Charlson et al. 1992). In nature, number concentrations of ice particles vary by orders of magnitude spatially in cloud systems. For all these reasons, it is sufficient to predict the order of magnitude of ice number concentrations correctly.

For four ICE-L flights, Pratt et al. (2009a, 2010a,b) and E10 hypothesized dominant types of active IN in view of the A-ATOFMS measurements of cloud-particle residues. Qualitatively, the composition of key species of active IN predicted by the EP includes those species hypothesized on each flight. A role for biological IN was predicted in two of the flights. Although Hoose et al. (2010) predicted an almost negligible fraction (about 10^{-7}) of all active IN that are PBAPs globally, their global model may have greatly underestimated it due to their treatment of bacterial ice nucleation using observations of IN activity of only one strain of Pseudomonas syringae (Ps) (Yankovsky et al. 1981), which was shown recently (Murray et al. 2012, their Fig. 14) to have an ice-nucleating efficiency at least 3–4 orders of magnitude lower than seen in most studies for other strains of Ps. To construct the EP, Ph08 used observations of very large samples of many natural strains of Ps (e.g., Hirano et al. 1985).

A striking result is the EP's prediction that black carbon is a major type of ice nucleus in clouds influenced by biomass-burning particles. Bingemer et al. (2012) observed the composition of IN sampled from the troposphere over Germany. Between 1% and 15% of active IN at −18°C were seen to be apparently pure particles of black carbon. This soot was likely anthropogenic and was not emitted by the volcanic eruptions being studied (Bingemer et al. 2012). Atmospheric cloud-ice residues were seen by Cozic et al. (2008) to be enriched with black carbon from biomass burning. Special conditions of temperature, oxygen availability, and fuel chemistry during combustion are needed for the black carbon to be ice nucleating. These conditions, and those during aging, control the organic coatings and hydrophilic nature of the black-carbon surface.

An extremely strong correlation of $r^2 > 0.99$ was observed by Twohy et al. (2010) between number concentrations of black carbon (SP2) and heterogeneously nucleated ice in ICE-L. This is consistent with a possible causal link between black carbon and ice. The SP2 accurately detects black carbon by measuring 1) absorption at 1064 nm, where organics generally do not absorb, and 2) incandescence at 4000 K and lack of volatility (organics do not incandesce). Twohy et al. (2010) observed a high, though weaker, correlation between concentrations of biomass-burning particles and ice ($r^2 > 0.91$). Internal mixing of most black carbon with other species in biomass-burning particles was seen by mass spectrometry in ICE-L (section 3a). If black carbon nucleated much ice in ICE-L clouds affected by carbonaceous aerosol, then this internal mixing would have caused the observed correlation with biomass-burning particles. If not, not.

It cannot be ruled out that another IN species (e.g., mineral dust, organics, inorganic salts), internally mixed with the black carbon, might have nucleated the observed ice. That would have caused both observed correlations (e.g., Stith et al. 2011). Generally, the lack of observation of apparently pure particles of black carbon among cloud-ice residues sampled by aircraft from cirrus (e.g., Cziczo et al. 2004) is explicable in terms of it either nucleating ice only when internally mixed with the identified biomass-burning particles or activating at higher humidities than other IN species. Indeed, the new version of the EP includes a higher value for black carbon of the humidity threshold ($S^X_{i,0}$) in subsaturated conditions at cold temperatures of cirrus compared to the other IN species.

Validation of the EP's treatment of biological ice nucleation is shown (section 3c) using coincident field observations of PBAP IN and PBAPs at SPL. Hence, the EP can be applied to study biosphere–atmosphere interactions and biological influences on clouds and precipitation (e.g. Phillips et al. 2009). Field observations (CR-AVE) of cirrus near the tropopause agree with predictions by the EP for soluble organic IN. Also, the latest laboratory data (e.g., K09, K10) compare adequately with the new EP for the other three IN groups. Its predicted active fraction has a similar order of magnitude to that observed. When the EP input is set to the size of hydrophilic black carbon studied recently, predicted and observed active fractions differ by less than a factor of 2. But for dust, and when size differences are accounted for, the prediction tends to be lower. This is expected, since surrogate dust from the ground is seen to have more active IN per unit surface area than the natural atmospheric dust treated by the EP at cold subzero temperatures (section 3b). To explain this, Ph08 hypothesized two types of atmospheric processing of IN aerosols during long-range transport:

- the more active IN are removed by ice nucleation from the aerosol population (microphysical processing), and
- coatings of (e.g., soluble) material on IN particles may modify their IN activity (chemical processing).

The present paper shows the apparent contrast in ice nucleation between surrogate and natural atmospheric aerosol is more pronounced at temperatures colder than about −35°C. This contrast is robust for many laboratory studies, though the atmospheric observations are few. When the same sample of soil dust is studied by the CFDC and AIDA chamber at similar conditions of humidity and temperature, the same IN concentration is observed (D11; Kanji et al. 2011) (e.g., compare observations of SD2 by K10 and F06 on Fig. 4). However, such comparisons between different measurement methods seem to have only been performed so far at temperatures warmer than about −40°C. The possibility of biases affecting field probes at colder temperatures cannot be completely ruled out.

There are two possible reasons for this apparent difference being greater at temperatures colder than −35°C. First, the atmospheric IN aerosols that activate at colder temperatures have fewer active sites per particle, so may be smaller and, hence, older when sampled. Thus, they may have had a longer history of atmospheric processing. Second, ice nucleation at temperatures warmer than about −35°C is seen to occur preferentially at humidities close to water saturation. In such conditions, IN activation by freezing is estimated to have little dependence on soluble coatings, owing to dilution of solute (Ph08; see also Fig. 4b) (Sullivan et al. 2010a). At colder temperatures, nucleation of ice by deposition mode is inhibited by soluble coatings (e.g., Cziczo et al. 2009; Eastwood et al. 2009; Möhler et al. 2008; Sullivan et al. 2010a,b).

There is some uncertainty in field observations of atmospheric IN. For observations used to develop the EP, the CFDC did not sample aerosol particles >1.5–2.5 μm in diameter. From stochastic effects, there is a brief uncertain time delay between imposing constant conditions of temperature–humidity and the instant of activation of IN (Anderson and Hallett 1976; Kulkarni and Dobbie 2010) (section 1), followed by a known delay between activation and growth of ice to detectable sizes. The total delay might conceivably in some conditions (i.e., colder temperatures) cause undercounting of active IN by the CFDC. Yet Field et al. (2012) find good agreement between observed (CFDC) and modeled IN concentrations in mixed-phase wave clouds of ICE-L at temperatures colder than −24°C. It is consistent with the accuracy and residence time of the CFDC being adequate here.

Field probes counting IN have limited accuracy at the warmest subzero temperatures, where active IN are scarce. This, together with their lack of direct resolution of the activity of individual species of IN, has necessitated application of approximate thresholds for the onsets of freezing during supercooling. Such thresholds are artificial and do not have universally constant values. Their application for the EP effectively involves approximating the conditions in natural clouds by those for their measurement in the laboratory. In reality, observed thresholds vary with experimental conditions such as the time scale of measurement, the minimum active fraction for detection, and aerosol size (e.g., Kanji and Abbatt 2006). In the future, it may be discovered that certain types of aerosol are active as IN at temperatures warmer than the present estimates of onset thresholds, where their active fractions are currently not measurable. Yet any IN activity that is now scarcely detectable might be expected to have little impact on cloud-microphysical processes.

Inevitably, accuracy is limited also for the species-specific shifts of temperature applied here to modify the treatment of contact freezing, again because of the current paucity of available laboratory observations. Note that treatment of contact freezing in an atmospheric model cannot be done merely by using Eq. (3) for concentrations of active contact IN alone. It requires also the prediction of rates of their collection by thermophoresis, diffusiophoresis, and Brownian diffusion onto supercooled cloud droplets, as explained by Ph08. This in turn necessitates prediction of the in-cloud supersaturation and properties of cloud liquid.

Regarding implementation of the revised EP in atmospheric models, most atmospheric models do not yet treat PBAPs explicitly. Sources of organics are diverse, so the PBAP concentration may not be simply related to the total insoluble organic concentration. If any Xth group of aerosol is neither predicted by the atmospheric model nor observed, as often happens for PBAPs, then it is recommended that Ω_X be replaced by the constant value of $\Omega_{X,1,*}$. Another challenge when applying the EP is that, for IN activity of black carbon, a few parameters are still uncertain (e.g., P_s, F_{OC}, ...), determining Ξ. These need not be specified, however, if it is assumed that $\Xi = 1$ for ice-nucleating biomass-burning plumes and $\Xi = 0$ for freshly emitted urban fossil-fuel combustion. One then selects which of the two extremes is most applicable for a given simulation.

Our replacement of the insoluble organic group by a new PBAP group should not be taken as implying that nonbiological insoluble organics cannot nucleate ice. Some observations suggest that they can (e.g., Schnell and Vali 1972; Knopf et al. 2010; Conen et al. 2011). Their activity is not yet empirically quantified in a comprehensive way. If future laboratory observations confirm and quantify any ice-nucleating ability of nonbiological insoluble organics, then another new group to treat them specifically might conceivably be created in future versions of our scheme.

Indeed, new species of IN are still being discovered (e.g., Mu10). Not all types of IN in the troposphere are likely known and empirically quantified. More research is needed to confirm that, among biomass-burning plumes worldwide, black carbon is an IN species. Laboratory data about black carbon's ice nucleation at warm temperatures (>-30°C) and about soluble organic IN are scarce. The relation between P_s, F_{OC}, and black carbon's IN activity needs to be observed, especially at warm temperatures and for realistic types of aged soot. In future, by coupling chemistry and aerosol components with the EP in an atmospheric model, it may become possible to predict the surface polarity P_s and organic coverage F_{OC} of black carbon and its mixing states for various sources and aerosol ages. There has been progress in simulating soot's chemistry (e.g., Riemer et al. 2010; Zaveri et al. 2010). This might reveal how IN activity of carbonaceous plumes evolves during transport. For instance, an important and open question in climate change is whether black carbon in fossil-fuel pollution can become IN-active after aging during long-range transport around the globe. Our approach provides a framework for addressing it.

Equally, there is a need for continued acquisition of coincident field observations of IN activity, aerosol composition, and ASDs from the troposphere, especially at both onset and low temperature conditions. Future field campaigns similar to ICE-L, perhaps with aircraft observations of more wave clouds in the upper half of the mixed-phase region, will advance the modeling of heterogeneous ice nucleation. There is a need for size-resolved chemical composition of active IN and aerosols in ambient air to be observed in future campaigns, preferably with a mass spectrometer coupled to the field probe for measuring IN. This will allow better acuity of validation of ice nucleation schemes. (The code of the EP is freely available from the first author on request.)

Acknowledgments. This research was supported by two awards to the first author from the Office of Science (BER), U. S. Department of Energy (DoE) (Award DE-SC0002383) and the Physical and Dynamical Meteorology program of National Science Foundation (Award ATM-0852620), as well as by an award from BER/DoE to Professor A. Khain at Hebrew University of Jerusalem (DE-S0006788). The work is directly applicable to these awards, which concern modeling studies of aerosol–cold-cloud interactions and of influences from environmental

factors (e.g. dust loading) on lightning. The authors are grateful to personnel involved in the 2007 ICE-L campaign, as well as support from NSF and NCAR. K. A. Pratt and K. Prather acknowledge NSF for support of ICE-L (ATM-0650659), A-ATOFMS development (ATM-0321362), and a graduate research fellowship for K. A. Pratt. C. Twohy was funded through an NSF award (AGS-1005020). V. Phillips acknowledges the advice and codes from J. Kealy, J. Sun, S. Howell, and A. Clarke at the University of Hawaii at Manoa and from B. Murray at University of Leeds. P. J. DeMott acknowledges support from NSF (ATM-0611936 and ATM-0841602).

APPENDIX A

List of Symbols

TABLE A1. Symbols used in this paper, along with their descriptions and units.

Notation	Description	Units
BC	Inorganic black carbon	
BIO	PBAP (organic) material (includes non-C elements)	
D_X	Actual equivalent spherical diameter of aerosol in group X	m
$D_{g,X}$	Geometric mean of D_X in group X	m
DM	Dust and metallic aerosols	
f_c	Contribution from CFDC data to H_X	
F_{OC}	Fraction of surface area of black carbon particle coated by non-PBAP insoluble organic material	
$F_{OC,0}$	Low threshold of F_{OC} for ice nucleation by black carbon	
$F_{OC,1}$	High threshold of F_{OC} for ice nucleation by black carbon	
g_{glass}	Fraction of soluble organic (by number) that can be glassy	
$g_{X,0.1\rightarrow1}$	The number of particles in group X, relative to all aerosol particles, at dry diameters between 0.1 and 1 μm	
H_X	Fraction reducing IN activity at low S_i, warm T [introduced by Ph08, their Eqs. (11) and (12)]	
$n_{IN,1,*}$	Number mixing ratio (m.r.) of active IN aerosols (0.1–1 μm in dry diameter) in reference activity spectrum for water saturation in background-troposphere scenario	No. kg^{-1}
$n_{IN,X}$	Contribution to n_{IN} from aerosol group X	No. kg^{-1}
n_X	Number m.r. of particles in aerosol group X (not depleted by ice nucleation while inside cloud)	No. kg^{-1}
$n_{IN,solO,@}$	Number m.r. of active IN in soluble organic group in AIDA experiment (Mu10)	No. kg^{-1}
N_s	Number of insoluble particles immersed in a drop	
P	Probability that a drop freezes	
P_s	Polarity of BC surface (measure of its hydrophilicity)	No. H_2O monolayers
$P_{s,0}$	Low threshold of P_s for ice nucleation by black carbon	No. H_2O monolayer
$P_{s,1}$	High threshold of P_s for ice nucleation by black carbon	No. H_2O monolayer
s_i	Supersaturation of vapor with respect to ice [$s_i = 100\ (S_i - 1)$]	%
s_w	Supersaturation of vapor with respect to water	%
solO	Soluble organics	
S_i	Saturation ratio of vapor with respect to ice	
$S_{i,0}^X$	Threshold of S_i in H_X for group X	
S_i^w	Value of S_i at exact water saturation	
ΔS_i^X	Range in S_i for transition of H_X (replaces ΔS_i in expression for H_X from Ph08)	
T	Physical temperature of ambient air	°C
$T_{X,1}$	Colder threshold of T for onset of freezing (replaces −5°C in original expression for ξ from Ph08)	°C
$T_{X,2}$	Warmer threshold of T for onset of freezing (replaces −2°C in original expression for ξ from Ph08)	°C
T_0^X	Threshold of temperature in H_X for group X	°C
ΔT^X	Range of temperatures for onset of ice nucleation at humidities well below water saturation (replaces ΔT in expression for H_X from Ph08)	°C
$\Delta T_{CIN,X}$	Difference in freezing temperature between surface and bulk-water modes of any IN particle in group X (replaces ΔT_{CIN} of Ph08)	°C
$\Delta T_{onset,X}$	Difference in temperature of onset of freezing between surface and bulk-water modes by aerosol group X	°C
X	Label for insoluble aerosol group (DM, BC, BIO, solO)	
α_X	Fraction of $n_{IN,1,*}$ from IN activity of group X	
$\tilde{\alpha}_{BC}$	Value of α_{BC} for optimal black carbon ($\Xi = 1$)	
γ	Factor boosting IN concentration due to bulk-liquid modes	2

TABLE A1. (*Continued*)

Notation	Description	Units
$\delta_a^b(y, y_1, y_2)$	Cubic interpolation function equal to a at $y \leq y_1$ and to b for $y \geq y_2$, being interpolated in between, as defined by Ph08	
ζ	Ratio of number of active IN to dust surface area	No. m^{-2} (dust)
κ	Hygroscopicity parameter	
μ^*	Average number of IN activated per drop	
μ_X	Average number of ice embryos per aerosol particle	
$\xi(T)$	Fraction that is 0 for $T > T_{X,2}$ (°C) and 1 for $T < T_{X,1}$ (°C), being $\delta_1^0(T, T_{X,1}, T_{X,2})$ for $T_{X,1} < T < T_{X,2}$ (°C)	
Ξ	Fraction defining black carbon's propensity for ice nucleation	
φ	Integer number of active IN per drop	
ρ_X	Bulk density of aerosols	kg m^{-3}
$\rho_@$	Air density in AIDA chamber at 200 K (Mu10)	kg m^{-3}
σ_X	Standard deviation ratio of aerosols in group X	
θ_e	Equivalent potential temperature	K
Ω_X	"Ideal" total surface area of all aerosols > 0.1 μm In diameter from group X (not depleted by ice nucleation while inside cloud)	m^2 (aerosol) kg $(air)^{-1}$
$\Omega_{X,\text{int}}$	Interstitial component of Ω_X	m^2 (aerosol) kg $(air)^{-1}$
$\Omega_{X,1,*}$	Component of Ω_X in background-troposphere scenario (INSPECT) for aerosol diameters between 0.1 and 1 μm in group X	m^2 (aerosol) kg $(air)^{-1}$
$\Omega_{\text{solO},@}$	Component of Ω_X in AIDA experiment (Mu10) for aerosol diameters > 0.1 μm in group X = solO	m^2 (aerosol) kg $(air)^{-1}$

APPENDIX B

Estimate of Baseline Surface Area of PBAPs from Field Observations

The EP is based on an assumption of approximate proportionality between active IN concentrations and the surface area of aerosols in each group. This requires an estimate of the baseline value of surface area mixing ratio for each group from the field campaign, INSPECT, where IN and aerosol conditions were observed.

Since PBAPs were not measured directly during INSPECT itself, their baseline surface area is estimated from more recent field data as follows. During the first week of April 2008, PBAP concentrations were observed at the same location (SPL, Mt. Werner, Colorado) as the original field campaigns (INSPECT-1 and -2, SPL, November 2001 and April 2004) constraining the EP. In that week of 2008, PBAPs larger than 0.5 μm in diameter constituted about 77% (0.61 μg m^{-3}) of the total mass of particulate organic carbon particles < 10 μm in diameter (POC10 = 0.79 μg m^{-3}) (W09). An effective mean diameter of 1.26 μm is assumed for the PBAPS > 0.5 μm sampled at SPL, in view of observations of ASDs of PBAPs elsewhere (M95).

During INSPECT-1 and -2 a few years earlier, the total organic mass of aerosols smaller than 2.5 μm ("OC2") in diameter was observed (IMPROVE, Mt. Zirkel) to be about 0.44 μg m^{-3} on average, which compares with 0.69 μg m^{-3} for the first week of April 2008. Parsimoniously, it may be assumed that PBAPs with diameters larger than 0.5 μm have a mass concentration that has the same ratio with respect to OC2 during INSPECT as in April 2008 (SPL); in reality, this ratio varies with the seasonal cycles of emissions of PBAPs and of pollution. That assumption implies that PBAPs larger than 0.5 μm during INSPECT had an average content of 0.39 μg m^{-3}.

The bimodal ASD of PBAPs observed by M95 at such sizes was rescaled to fit this mass concentration estimated for INSPECT, 0.39 μg m^{-3}, at diameters greater than 0.5 μm. An average surface area of $\Omega_{\text{BIO},1,*} = 8.9 \times 10^{-7}$ m^2 kg^{-1} is obtained for INSPECT-1 and -2. A bulk density of PBAPs of 1000 kg m^{-3} (M00) is assumed. This is an estimate for the same location and mostly a similar month as the CFDC measurements (INSPECT) constraining the EP, albeit from a different year. There is uncertainty noted by W09 about the mass fraction and ASD parameters assumed, which were not measured and must vary especially over altitude.

APPENDIX C

Observations of Factors Controlling the Ice-Nucleating Ability of Soot

Observations suggest that at least three crucial factors control the ice-nucleating ability of black carbon. They are hydrophilic chemical groups bonded to its surface, coatings by organic material, and the morphology of black carbon. The following discussion of the literature

about these three factors has informed our modification to the EP (section 2e).

a. Role of hydrophilic surface with polarity

K09 observed that when the black-carbon surface is ''intrinsically hydrophilic'' it has a greater ice-nucleating ability. The surface can be intrinsically hydrophilic by having intermediate polarity and sufficient numbers of oxygen-containing functional groups attached. Such functional groups are assumed to provide active sites for ice nucleation. Black carbon with an intrinsically hydrophobic surface was seen not to nucleate ice significantly.

Generally for IN, oxygen-containing functional groups can promote hydrogen bonding with water molecules and ice nucleation (Edwards and Evans 1971). They favor formation of an icelike molecular lattice of water on the IN material. This notion was corroborated for organic IN at extremely cold temperatures by Schill and Tolbert (2012). A higher O:C ratio was seen to promote ice nucleation.

Surface polarity of black carbon P_s may be defined as the number of water monolayers adsorbed onto it when exposed to the vapor at 50% relative humidity (Popovicheva et al. 2008a,b) after all soluble material has been washed away. Immersing hydrophobic ''thermal soot,'' which did not initially nucleate much ice, in concentrated sulphuric acid for a month increased P_s. It became ''thermal oxidized soot'' that did nucleate ice at temperatures below −40°C (K09). By contrast, soluble coatings conferred only hygroscopicity and CCN activity without directly boosting IN activity; they could even interfere with it by leading to the onset of homogeneous freezing at expected conditions for water dissolved in the coatings. Such hygroscopicity from soluble coatings is distinct from the intrinsic hydrophilicity of the black-carbon surface measured by P_s.

Petters et al. (2009a) observed a positive correlation between IN activity and average hygroscopicity of all particles in any biomass-burning plume. Field observations reveal thicker soluble (volatile) coatings and a greater hygroscopicity κ of soot-containing particles in biomass-burning plumes compared to those in fresh urban fossil-fuel pollution (Schwarz et al. 2008). If gas-particle partitioning and/or heterogeneous reactions, which generate soluble coatings on black carbon, also create oxygen-containing active sites on its surface, then this would boost both P_s and IN activity (freezing) of black carbon from biomass burning. Such reactions may stem from sulphuric acid coatings or aqueous-phase chemistry, and some may involve ozone and OH. They may occur near the combustion or slowly during long-range transport (e.g., Pagels et al. 2009; Moffet and Prather 2009; Riemer et al. 2010).

b. Role of organic coatings

Fresh black carbon from fossil-fuel combustion, coated with organic material, was studied in the AIDA chamber (Möhler et al. 2005b; C11). C11 observed that soot-containing particles with 5% organic content were efficient IN at about −45°C, activating at humidities below the threshold for homogeneous aerosol freezing. But they nucleated ice only at humidities far above this threshold when organic contents were 30% or 70%. So, their organic coatings had little solubility. Time delays between scattering and incandescence in the SP2 implied thick coatings encasing the black carbon for the 30% and 70% contents. Möhler et al. (2005b) observed a similar contrast for 16% and 40% organic contents at 207 K, with IN activity only for the former. C11 suggest that organic contents exceeding 10%–20% switch the nucleation mode from deposition to freezing, which requires higher humidities.

Similarly, at warmer temperatures (near −30°C) the IN activity and average organic content of fresh biomass-burning plumes are strongly anticorrelated (Petters et al. 2009a). Knopf et al. (2010) did not observe inhibition of IN activity by organic coatings among carbonaceous particles that were apparently anthropogenic and were sampled from Mexico City. Yet it is unclear whether the coatings were insoluble. Hence, for warm subzero temperatures (above −40°C), we hypothesize that any insoluble organic coatings smothering the black carbon will inhibit heterogeneous freezing. This inhibition of ice nucleation must be governed by F_{OC}, the fractional coverage of black-carbon surface by insoluble organics. [The hypothesized impact of organic coatings is specific to black carbon, as inclusions of organic material in organic-dominated biomass-burning particles were inferred to trigger ice nucleation in another study (Stith et al. 2011).]

In African plumes from burning of savannah, contrasting types of carbonaceous particle were observed (Pósfai et al. 2003): 1) organics, 2) tar balls (organic-like), and 3) black carbon. The particles would become coated with sulfate and volatile organics by cocondensation during transport. But the black carbon would only become internally mixed with insoluble organics by agglomeration, forming loose aggregates. This suggests $F_{OC} \approx 0$ for black carbon from biomass burning, despite the greater mass of refractory and insoluble organics (Mayol-Bracero et al. 2002; Clarke et al. 2007) in the plume.

Early coatings of insoluble organics near the combustion source may be critical for F_{OC}. For contact with the black carbon, they must be deposited before the (secondary) soluble material. Fresh urban pollution

from fossil-fuel combustion contains organic material that is mostly insoluble, has low polarity, and is poorly oxygenated (Weber et al. 2007), from a low air–fuel ratio. The opposite is true for fresh biomass-burning plumes (Mayol-Bracero et al. 2002; Reid et al. 2005). In Mexico City, most organic material (79%) from fossil-fuel combustion was insoluble, whereas most was soluble from biomass burning (Aiken et al. 2010). Soluble organics in fossil-fuel pollution are mostly only acquired later by secondary processes. This all suggests $F_{OC} \approx 1$ for freshly emitted fossil-fuel pollution.

In reality, ice nucleation can sometimes be modified by soluble organics for certain carbonaceous particles (e.g., Petters et al. 2009a). Laboratory data to quantify this effect are scarce, however.

c. *Role of black carbon morphology and crystallographic structure*

Soot–sulfate particles from biomass burning may have more ordered microstructures of carbon atoms than from fossil-fuel combustion (Pósfai et al. 1999, 2003). Combustion temperature controls such order (Li et al. 2011). Yet the effect for soot's ice nucleation is uncertain.

REFERENCES

Adachi, K., S. H. Chung, and P. R. Buseck, 2010: Shapes of soot aerosol particles and implications for their effects on climate. *J. Geophys. Res.,* **115,** D15206, doi:10.1029/2009JD012868.

Aiken, A. C., and Coauthors, 2010: Mexico City aerosol analysis during MILAGRO using high resolution aerosol mass spectrometry at the urban supersite (T0)—Part 2: Analysis of the biomass burning contribution and the non-fossil carbon fractions. *Atmos. Chem. Phys.,* **10,** 5315–5341.

Anderson, J., and J. Hallett, 1976: Supersaturation and time dependence of ice nucleation from the vapor on single crystal substrates. *J. Atmos. Sci.,* **33,** 822.

Ansmann, A., and Coauthors, 2008: Influence of Saharan dust on cloud glaciation in southern Morocco during the Saharan Mineral Dust Experiment. *J. Geophys. Res.,* **113,** D04210, doi:10.1029/2007JD008785.

Archuleta, C. M., P. J. DeMott, and S. M. Kreidenweis, 2005: Ice nucleation by surrogates for atmospheric mineral dust and mineral dust/sulfate particles at cirrus temperatures. *Atmos. Chem. Phys.,* **5,** 2617–2634.

Baumgardner, D., R. Subramanian, C. Twohy, J. Stith, and G. Kok, 2008: Scavenging of black carbon by ice crystals over the northern Pacific. *Geophys. Res. Lett.,* **35,** L22815, doi:10.1029/2008GL035764.

Baustian, K. J., M. E. Wise, and M. A. Tolbert, 2011: Depositional ice nucleation on solid ammonium sulfate and glutaric acid particles. *Atmos. Chem. Phys.,* **10,** 2307–2317.

Bingemer, H., and Coauthors, 2012: Atmospheric ice nuclei in the Eyjafjallajökull volcanic ash plume. *Atmos. Chem. Phys.,* **12,** 857–867, doi:10.5194/acp-12-857-2012.

Bowers, R. M., C. L. Lauber, C. Wiedinmyer, M. Hamady, A. G. Hallar, R. Fall, R. Knight, and N. Fierer, 2009: Characterization of airborne microbial communities at a high-elevation site and their potential to act as atmospheric ice nuclei. *Appl. Environ. Microbiol.,* **75,** 5121–5130, doi:10.1128/AEM.00447-09.

Broadley, S. L., B. J. Murray, R. J. Herbert, J. D. Atkinson, S. Dobbie, T. L. Malkin, E. Condliffe, and L. Neve, 2012: Immersion mode heterogeneous ice nucleation by an illite rich powder representative of atmospheric mineral dust. *Atmos. Chem. Phys.,* **12,** 287–307.

Charlson, R. J., S. E. Schwartz, J. M. Hales, R. D. Cess, J. A. Coakley, J. E. Hansen, and D. J. Hofmann, 1992: Climate forcing by anthropogenic aerosol. *Science,* **255,** 423–430.

Chernoff, D. I., and A. K. Bertram, 2010: Effects of sulfate coatings on the ice nucleation properties of a biological ice nucleus and several types of minerals. *J. Geophys. Res.,* **115,** D20205, doi:10.1029/2010JD014254.

Clarke, A. D., and Coauthors, 2004: Size distributions and mixtures of dust and black carbon aerosol in Asian outflow: Physiochemistry and optical properties. *J. Geophys. Res.,* **109,** D15S09, doi:10.1029/2003JD004378.

——, and Coauthors, 2007: Biomass burning and pollution aerosol over North America: Organic components and their influence on spectral optical properties and humidification response. *J. Geophys. Res.,* **112,** D12S18, doi:10.1029/2006JD007777.

Conen, F., C. E. Morris, J. Leifeld, M. V. Yakutin, and C. Alewell, 2011: Biological residues define the ice nucleation properties of soil dust. *Atmos. Chem. Phys,* **11,** 9643–9648.

Connolly, P. J., O. Möhler, P. R. Field, H. Saathoff, R. Burgess, T. Choularton, and M. Gallagher, 2009: Studies of heterogeneous freezing by three different desert dust samples. *Atmos. Chem. Phys.,* **9,** 2805–2824.

Cooper, W. A., 1980: A method of detecting contact ice nuclei using filter samples. Preprints, *Eighth Int. Conf. on Cloud Physics,* Clermont-Ferrand, France, IUGG, 665–668.

Cozic, J., S. Mertes, B. Verheggen, D. J. Cziczo, S. J. Gallavardin, S. Walter, U. Baltensperger, and E. Weingartner, 2008: Black carbon enrichment in atmospheric ice particle residuals observed in lower tropospheric mixed phase clouds. *J. Geophys. Res.,* **113,** D15209, doi:10.1029/2007JD009266.

Crawford, I., and Coauthors, 2011: Studies of propane flame soot acting as heterogeneous ice nuclei in conjunction with single particle soot photometer measurements. *Atmos. Chem. Phys.,* **11,** 9549–9561.

Cziczo, D. J., D. M. Murphy, P. K. Hudson, and D. S. Thomson, 2004: Single particle measurements of the chemical composition of cirrus ice residue during CRYSTAL-FACE. *J. Geophys. Res.,* **109,** D04201, doi:10.1029/2003JD004032.

——, K. D. Froyd, S. J. Gallavardin, O. Moehler, S. Benz, H. Saathoff, and D. M. Murphy, 2009: Deactivation of ice nuclei due to atmospherically relevant surface coatings. *Environ. Res. Lett.,* **4,** 044013, doi:10.1088/1748-9326/4/4/044013.

DeMott, P. J., 1990: An exploratory study of ice nucleation. *J. Appl. Meteor.,* **29,** 1072–1080.

——, Y. Chen, S. M. Kreidenweis, D. C. Rogers, and D. Eli Sherman, 1999: Ice formation by black carbon particles. *Geophys. Res. Lett.,* **26,** 2429–2432.

——, D. J. Cziczo, A. J. Prenni, D. M. Murphy, S. M. Kreidenweis, D. S. Thomson, R. Borys, and D. C. Rogers, 2003a: Measurements of the concentration and composition of nuclei for cirrus formation. *Proc. Natl. Acad. Sci. USA,* **100,** 14 655–14 660.

——, K. Sassen, M. R. Poellot, D. Baumgardner, D. C. Rogers, S. D. Brooks, A. J. Prenni, and S. M. Kreidenweis, 2003b: African dust aerosols as atmospheric ice nuclei. *Geophys. Res. Lett.,* **30,** 1732, doi:10.1029/2003GL017410.

——, and Coauthors, 2011: Resurgence in ice nucleation research. *Bull. Amer. Meteor. Soc.,* **92,** 1623–1635.

Diehl, K., and S. K. Mitra, 1998: A laboratory study of the effects of a kerosene-burner exhaust on ice nucleation and the evaporation rate of ice crystals. *Atmos. Environ.,* **32,** 3145–3151.

Durant, A. J., and R. A. Shaw, 2005: Evaporation freezing by contact nucleation inside-out. *Geophys. Res. Lett.,* **32,** L20814, doi:10.1029/2005GL024175.

Eastwood, M. L., S. Cremel, M. Wheeler, B. J. Murray, E. Girard, and A. K. Bertram, 2009: Effects of sulfuric acid and ammonium sulfate coatings on the ice nucleation properties of kaolinite particles. *Geophys. Res. Lett.,* **36,** L02811, doi:10.1029/2008GL035997.

Edwards, G. R., and L. F. Evans, 1971: The mechanism of activation of ice nuclei. *J. Atmos. Sci.,* **28,** 1443–1447.

Eidhammer, T., P. J. DeMott, and S. M. Kreidenweis, 2009: A comparison of heterogeneous ice nucleation parameterizations using a parcel model framework. *J. Geophys. Res.,* **114,** D06202, doi:10.1029/2008JD011095.

——, and Coauthors, 2010: Ice initiation by aerosol particles: Measured and predicted ice nuclei concentrations versus measured ice crystal concentrations in an orographic wave cloud. *J. Atmos. Sci.,* **67,** 2417–2436.

Field, P. R., O. Möhler, P. Connolly, M. Kramer, R. Cotton, A. J. Heymsfield, M. Schnaiter, and H. Saathoff, 2006: Some ice nucleation characteristics of Asian and Saharan desert dust. *Atmos. Chem. Phys.,* **6,** 1539–1577.

——, A. J. Heymsfield, B. J. Shipway, P. J. DeMott, K. A. Pratt, D. C. Rogers, J. Stith, and K. A. Prather, 2012: Ice in Clouds Experiment–Layer Clouds. Part II: Testing characteristics of heterogeneous ice formation in lee wave clouds. *J. Atmos. Sci.,* **69,**1066–1079.

Fornea, A. P., S. D. Brooks, J. B. Dooley, and A. Saha, 2009: Heterogeneous freezing of ice on atmospheric aerosols containing ash, soot, and soil. *J. Geophys. Res.,* **114,** D13201, doi:10.1029/2009JD011958.

Forster, P., and Coauthors, 2007: Changes in atmospheric constituents and in radiative forcing. *Climate Change 2007: The Physical Science Basis,* S. Solomon et al., Eds., Cambridge University Press, 129–234.

Froyd, K. D., D. M. Murphy, T. J. Sanford, D. S. Thomson, J. C. Wilson, L. Pfister, and L. Lait, 2009: Aerosol composition of the tropical upper troposphere. *Atmos. Chem. Phys.,* **9,** 4363–4385.

——, ——, P. Lawson, D. Baumgardner, and R. L. Herman, 2010: Aerosols that form subvisible cirrus at the tropical tropopause. *Atmos. Chem. Phys.,* **10,** 209–218.

Gallavardin, S. J., K. D. Froyd, U. Lohmann, O. Moehler, D. M. Murphy, and D. Cziczo, 2008: Single particle laser mass spectrometry applied to differential ice nucleation experiments at the AIDA chamber. *Aerosol Sci. Technol.,* **42,** 773–791.

Garcia, E., T. C. J. Hill, A. J. Prenni, P. J. DeMott, G. D. Franc, and S. M. Kreidenweis, 2012: Biogenic ice nuclei in boundary layer air over two U.S. High Plains agricultural regions. *J. Geophys. Res.,* **117,** D18209, doi:10.1029/2012JD018343.

Gokhale, N. R., and J. Goold, 1968: Droplet freezing by surface nucleation. *J. Appl. Meteor.,* **7,** 870–874.

Griffin, D. W., V. H. Garrison, J. R. Herman, and E. A. Shinn, 2001: African desert dust in the Caribbean atmosphere: Microbiology and public health. *Aerobiologia,* **17,** 203–213, doi:10.1023/A:1011868218901.

Gross, D. C., Y. S. Cody, E. L. Proebsting, G. K. Radamaker, and R. A. Spotts, 1983: Distribution, population dynamics, and characteristics of ice nucleation-active bacteria in deciduous fruit tree orchards. *Appl. Environ. Microbiol.,* **46,** 1370–1379.

Gurganus, C., A. B. Kostinski, and R. A. Shaw, 2011: Fast imaging of freezing drops: No preference for nucleation at the contact line. *J. Phys. Chem. Lett.,* **2,** 1449–1454, doi:10.1021/jz2004528.

Hallett, J., B. Gardiner, J. Hudson, and F. Rogers, 1986: Cloud condensation and ice nucleation of a range of carbonaceous aerosols. Preprints, *Conf. on Cloud Physics,* Vol. 2, Snowmass, CO, Amer. Meteor. Soc., 9–12.

Hirano, S. S., L. S. Baker, and C. D. Upper, 1985: Ice nucleation temperature of individual leaves in relation to population sizes of ice nucleation active bacteria and frost injury. *Plant Physiol.,* **77,** 259–265.

Hoose, C., and O. Möhler, 2012: Heterogeneous ice nucleation on atmospheric aerosols: A review of results from laboratory experiments. *Atmos. Chem. Phys. Discuss.,* **12,** 12 531–12 621.

——, J. E. Kristjansson, J.-P. Chen, and A. Hazra, 2010: A classical-theory-based parameterization of heterogeneous ice nucleation by mineral dust, soot, and biological particles in a global climate model. *J. Atmos. Sci.,* **67,** 2483–2503.

Kanji, Z. A., and J. P. D. Abbatt, 2006: Laboratory studies of ice formation via deposition mode nucleation onto mineral dust and n-hexane soot samples. *J. Geophys. Res.,* **111,** D16204, doi:10.1029/2005JD006766.

——, P. J. DeMott, O. Möhler, and J. P. D. Abbatt, 2011: Results from the University of Toronto continuous flow diffusion chamber at ICIS 2007: Instrument intercomparison and ice onsets for different aerosol types. *Atmos. Chem. Phys.,* **11,** 31–41, doi:10.5194/acp-11-31-2011.

Klein, H., and Coauthors, 2010: Saharan dust and ice nuclei over Central Europe. *Atmos. Chem. Phys.,* **10,** 10 211–10 221.

Knopf, D. A., B. Wang, A. Laskin, R. C. Moffet, and M. K. Gilles, 2010: Heterogeneous nucleation of ice on anthropogenic organic particles collected in Mexico City. *Geophys. Res. Lett.,* **37,** L11803, doi:10.1029/2010GL043362.

Koehler, K. A., S. M. Kreidenweis, P. J. DeMott, A. J. Prenni, and M. D. Petters, 2007: Potential impact of Owens (dry) Lake dust on warm and cold cloud formation. *J. Geophys. Res.,* **112,** D12210, doi:10.1029/2007JD008413.

——, and Coauthors, 2009: Cloud condensation nuclei and ice nucleation activity of hydrophobic and hydrophilic soot particles. *Phys. Chem. Chem. Phys.,* **11,** 7906–7920, doi:10.1039/b905334b.

——, S. M. Kreidenweis, P. J. DeMott, M. D. Petters, A. J. Prenni, and O. Möhler, 2010: Laboratory investigations of the impact of mineral dust aerosol on cold cloud formation. *Atmos. Chem. Phys.,* **10,** 11 955–11 968.

Korolev, A., 2007: Limitations of the Wegener–Bergeron–Findeisen mechanism in the evolution of mixed-phase clouds. *J. Atmos. Sci.,* **64,** 3372–3375.

——, and I. P. Mazin, 2003: Supersaturation of water vapor in clouds. *J. Atmos. Sci.,* **60,** 2957–2974.

——, and G. A. Isaac, 2005: Shattering during sampling by OAPs and HVPS. Part I: Snow particles. *J. Atmos. Oceanic Technol.,* **22,** 528–542.

Kulkarni, G., and S. Dobbie, 2010: Ice nucleation properties of mineral dust particles: Determination of onset RH_i, IN active fraction, nucleation time-lag, and the effect of active sites on contact angles. *Atmos. Chem. Phys.,* **10,** 95–105, doi:10.5194/acp-10-95-2010.

Levin, Z., and S. A. Yankofsky, 1983: Contact versus immersion freezing of freely suspended droplets by bacterial ice nuclei. *J. Climate Appl. Meteor.,* **22,** 1964–1966.

Li, Z., C. Song, J. Song, G. Lv, S. Dong, and Z. Zhao, 2011: Evolution of the nanostructure, fractal dimension and size of incylinder soot during diesel combustion process. *Combust. Flame,* **158,** 1624–1630.

Lindow, S. E., 1982: Population dynamics of epiphytic ice nucleation active bacteria on frost sensitive plants and frost control by means of antagonistic bacteria. *Plant Cold-Hardiness and Freezing Stress,* P. H. Li and A. Sakai, Eds., Vol. 2, Academic Press, 395–416.

——, D. C. Arny, and C. D. Upper, 1978: Distribution of ice nucleation-active bacteria on plants in nature. *Appl. Environ. Microbiol.,* **36,** 831–838.

——, ——, and ——, 1982: Bacterial ice nucleation: A factor in frost injury to plants. *Plant Physiol.,* **70,** 1084–1089.

——, E. Lahue, A. G. Govindarajan, N. J. Panopoulos, and D. Gies, 1989: Localization of ice nucleation activity and the iceC gene product in Pseudomonas syringae and Escherichia coli. *Mol. Plant-Microbe Interact.,* **2,** 262–272.

Maki, L. R., E. L. Galyan, M. M. Chang-Chien, and D. R. Caldwell, 1974: Ice nucleation induced by Pseudomonas Syringae. *Appl. Environ. Microbiol.,* **28,** 456–459.

Marcolli, C., S. Gedamke, T. Peter, and B. Zobrist, 2007: Efficiency of immersion mode ice nucleation on surrogates of mineral dust. *Atmos. Chem. Phys.,* **7,** 5081–5091.

Mason, B. J., and J. Maybank, 1958: Ice-nucleating properties of some natural mineral dusts. *Quart. J. Roy. Meteor. Soc.,* **84,** 235–241.

Matthias-Maser, S., and R. Jaenicke, 1995: The size distribution of primary biological aerosol particles with radii >0.2 μm in an urban/rural influenced region. *Atmos. Res.,* **39,** 279–286.

——, B. Bogs, and R. Jaenicke, 2000: The size distribution of primary biological aerosol particles in cloud water on the mountain Kleiner Feldberg/Taunus (FRG). *Atmos. Res.,* **54,** 1–13.

Mayol-Bracero, O. L., P. Guyon, B. Graham, M. O. Andreae, P. Artaxo, M. C. Facchini, S. Decesari, and S. Fuzzi, 2002: Water-soluble organic compounds in biomass burning aerosols over Amazonia: 2. Apportionment of the chemical composition and importance of the polyacidic fraction. *J. Geophys. Res.,* **107,** 8091, doi:10.1029/2001JD000522.

McConnell, C. L., and Coauthors, 2008: Seasonal variations of the physical and optical characteristics of Saharan dust: Results from the Dust Outflow and Deposition to the Ocean (DODO) experiment. *J. Geophys. Res.,* **113,** D14S05, doi:10.1029/2007JD009606.

Meyers, M. P., P. J. DeMott, and W. R. Cotton, 1992: New primary ice-nucleation parameterizations in an explicit cloud model. *J. Appl. Meteor.,* **31,** 708–720.

Ming, Y., V. Ramaswamy, L. J. Donner, and V. T. J. Phillips, 2006: A robust parameterization of cloud droplet activation. *J. Atmos. Sci.,* **63,** 1348–1356.

Moffet, R. C., and K. A. Prather, 2009: In-situ measurements of the mixing state and optical properties of soot with implications for radiative forcing estimates. *Proc. Natl. Acad. Sci. USA,* **106,** 11 872–11 877.

Möhler, O., and Coauthors, 2005a: Effect of sulfuric acid coating on heterogeneous ice nucleation by soot aerosol particles. *J. Geophys. Res.,* **110,** D11210, doi:10.1029/2004JD005169.

——, C. Linke, H. Saathoff, M. Schnaiter, R. Wagner, U. Schurath, A. Mangold, and M. Kramer, 2005b: Ice nucleation on flame soot aerosol of different organic carbon content. *Meteor. Z.,* **14,** 477–484.

——, and Coauthors, 2006: Efficiency of the deposition mode ice nucleation on mineral dust particles. *Atmos. Chem. Phys. Discuss.,* **6,** 1539–1577.

——, P. J. DeMott, G. Vali, and Z. Levin, 2007: Microbiology and atmospheric processes: The role of biological particles in cloud physics. *Biogeosciences,* **4,** 1059–1071.

——, and Coauthors, 2008: The effect of organic coating on the heterogeneous ice nucleation efficiency of mineral dust aerosols. *Environ. Res. Lett.,* **3,** 1–8.

Morris, C. E., D. G. Georgakopoulos, and D. C. Sands, 2004: Ice nucleation active bacteria and their potential role in precipitation. *J. Phys. IV France,* **121,** 87–103.

Murray, B. J., and Coauthors, 2010: Heterogeneous nucleation of ice particles on glassy aerosols under cirrus conditions. *Nat. Geosci.,* **3,** 233–237, doi:10.1038/ngeo817.

——, S. L. Broadley, T. W. Wilson, J. D. Atkinson, and R. H. Wills, 2011: Heterogeneous freezing of water droplets containing kaolinite particles. *Atmos. Chem. Phys.,* **11,** 4191–4207.

——, D. O'Sullivan, J. D. Atkinson, and M. E. Webb, 2012: Ice nucleation by particles immersed in supercooled cloud droplets. *Chem. Soc. Rev.,* **41,** 6519–6554.

Niedermeier, D., R. A. Shaw, S. Hartmann, H. Wex, T. Clauss, J. Voigtlnder, and F. Stratmann, 2011: Heterogeneous ice nucleation: Exploring the transition from stochastic to singular freezing behavior. *Atmos. Chem. Phys.,* **11,** 8767–8775, doi:10.5194/acp-11-8767-2011.

Niemand, M., and Coauthors, 2012: A particle-surface-area-based parameterization of immersion freezing on desert dust particles. *J. Atmos. Sci.,* **69,** 3077–3092.

Noone, K. J., J. A. Ogren, and R. J. Charlson, 1988: Design and calibration of a counterflow virtual impactor for sampling of atmospheric fog and cloud droplets. *Aerosol Sci. Technol.,* **8,** 235–244.

Pagels, J., A. F. Khalizov, P. H. McMurry, and R. Y. Zhang, 2009: Processing of soot by controlled sulphuric acid and water condensation-mass and mobility relationship. *Aerosol Sci. Technol.,* **43,** 629–640.

Petters, M. D., and S. M. Kreidenweis, 2007: A single parameter representation of hygroscopic growth and cloud condensation nucleus activity. *Atmos. Chem. Phys.,* **7,** 1961–1971.

——, and Coauthors, 2009a: Ice nuclei emissions from biomass burning. *J. Geophys. Res.,* **114,** D07209, doi:10.1029/2008JD011532.

——, C. M. Carrico, S. M. Kreidenweis, A. J. Prenni, P. J. DeMott, J. L. Collett Jr., and H. Moosmüller, 2009b: Cloud condensation nucleation activity of biomass burning aerosol. *J. Geophys. Res.,* **114,** D22205, doi:10.1029/2009JD012353.

Phillips, V. T. J., L. J. Donner, and S. T. Garner, 2007: Nucleation processes in deep convection simulated by a cloud-system-resolving model with double-moment bulk microphysics. *J. Atmos. Sci.,* **64,** 738–761.

——, P. J. DeMott, and C. Andronache, 2008: An empirical parameterization of heterogeneous ice nucleation for multiple chemical species of aerosol. *J. Atmos. Sci.,* **65,** 2757–2783.

——, and Coauthors, 2009: Potential impacts from biological aerosols on ensembles of continental clouds simulated numerically. *Biogeosciences,* **6,** 1–28.

Pitter, R. L., and H. R. Pruppacher, 1973: A wind tunnel investigation of freezing of small water drops falling at terminal velocity in air. *Quart. J. Roy. Meteor. Soc.,* **99,** 540–550.

Popovicheva, O., E. Kireeva, N. Persiantseva, T. Khoklova, N. Shonija, V. Tishkova, and B. Demirdjian, 2008a: Effect of

soot on immersion freezing of water and possible atmospheric implications. *Atmos. Res.,* **90** (2–4), 326–337.

——, and Coauthors, 2008b: Water interaction with hydrophobic and hydrophilic soot particles. *Phys. Chem. Chem. Phys.,* **10,** 2332–2344, doi:10.1039/B718944N.

Pósfai, M., J. R. Anderson, P. R. Buseck, and H. Sievering, 1999: Soot and sulfate aerosol particles in the remote marine troposphere. *J. Geophys. Res.,* **104** (D17), 21 685–21 693.

——, R. Simonics, J. Li, P. V. Hobbs, and P. R. Buseck, 2003: Individual aerosol particles from biomass burning in southern Africa: 1. Compositions and size distributions of carbonaceous particles. *J. Geophys. Res.,* **108,** 8483, doi:10.1029/2002JD002291.

Pratt, K. A., and K. A. Prather, 2010: Aircraft measurements of vertical profiles of aerosol mixing states. *J. Geophys. Res.,* **115,** D11305, doi:10.1029/2009JD013150.

——, and Coauthors, 2009a: In situ detection of biological particles in cloud ice-crystals. *Nat. Geosci.,* **2,** 398–401, doi:10.1038/ngeo521.

——, and Coauthors, 2009b: Development and characterization of an aircraft aerosol time-of-flight mass spectrometer. *Anal. Chem.,* **81,** 1792–1800.

——, and Coauthors, 2010a: Observation of playa salts as nuclei in orographic wave clouds. *J. Geophys. Res.,* **115,** D15301, doi:10.1029/2009JD013606.

——, and Coauthors, 2010b: In situ chemical characterization of aged biomass-burning aerosols impacting cold wave clouds. *J. Atmos. Sci.,* **67,** 2451–2468.

——, and Coauthors, 2011: Flight-based chemical characterization of biomass burning aerosols within two prescribed burn smoke plumes. *Atmos. Chem. Phys.,* **11,** 12 549–12 565, doi:10.5194/acp-11-12549-2011.

Prenni, A. J., and Coauthors, 2009: Relative roles of biogenic emissions and Saharan dust as ice nuclei in the Amazon basin. *Nat. Geosci.,* **2,** 402–405, doi:10.1038/ngeo517.

Pruppacher, H. R., and J. D. Klett, 1997: *Microphysics of Clouds and Precipitation.* Atmospheric and Oceanographic Sciences Library, Vol. 18, Springer, 976 pp.

Ramanathan, V., P. J. Crutzen, J. T. Kiehl, and D. Rosenfeld, 2001: Aerosols, climate, and the hydrological cycle. *Science,* **294,** 2119–2124, doi:10.1126/science.1064034.

Reid, J. S., R. Koppmann, T. F. Eck, and D. P. Eleuterio, 2005: A review of biomass burning emissions. Part II: Intensive physical properties of biomass burning particles. *Atmos. Chem. Phys.,* **5,** 799–825.

Richardson, M. S., and Coauthors, 2007: Measurements of heterogeneous ice nuclei in the western United States in springtime and their relation to aerosol characteristics. *J. Geophys. Res.,* **112,** D02209, doi:10.1029/2006JD007500.

——, P. J. DeMott, S. M. Kreidenweis, M. D. Petters, and C. M. Carrico, 2010: Observations of ice nucleation by ambient aerosol in the homogeneous freezing regime. *Geophys. Res. Lett.,* **37,** L04806, doi:10.1029/2009GL041912.

Riemer, N., M. West, R. Zaveri, and R. Easter, 2010: Estimating black carbon aging time-scales with a particle-resolved aerosol model. *J. Aerosol Sci.,* **41,** 143–158.

Roberts, P., and J. Hallett, 1968: A laboratory study of the ice nucleating properties of some mineral particulates. *Quart. J. Roy. Meteor. Soc.,* **94,** 25–34.

Rogers, D. C., P. J. DeMott, S. M. Kreidenweis, and Y. Chen, 2001: A continuous-flow diffusion chamber for airborne measurements of ice nuclei. *J. Atmos. Oceanic Technol.,* **18,** 725–741.

Sassen, K., P. J. DeMott, J. M. Prospero, and M. R. Poellot, 2003: Saharan dust storms and indirect aerosol effects on clouds: CRYSTAL-FACE results. *Geophys. Res. Lett.,* **30,** 1633, doi:10.1029/2003GL017371.

Schill, G. P., and M. A. Tolbert, 2012: Depositional ice nucleation on monocarboxylic acids: Effect of the O:C ratio. *J. Phys. Chem.,* **116A,** 6817–6822.

Schnell, R. C., and G. Vali, 1972: Atmospheric ice nuclei from decomposing vegetation. *Nature,* **236,** 163–165.

——, and ——, 1976: Biogenic ice nuclei: Part I. Terrestrial and marine sources. *J. Atmos. Sci.,* **33,** 1554–1564.

Schwarz, J. P., and Coauthors, 2006: Single-particle measurements of midlatitude black carbon and light-scattering aerosols from the boundary layer to the lower stratosphere. *J. Geophys. Res.,* **111,** D16207, doi:10.1029/2006JD007076.

——, and Coauthors, 2008: Measurement of the mixing state, mass, and optical size of individual black carbon particles in urban and biomass burning emissions. *Geophys. Res. Lett.,* **35,** L13810, doi:10.1029/2008GL033968.

Shaw, R. A., A. J. Durant, and Y. Mi, 2005: Heterogeneous surface crystallization observed in undercooled water. *J. Phys. Chem.,* **109B,** 9865–9868.

Shilling, J. E., T. J. Fortin, and M. A. Tolbert, 2006: Depositional ice nucleation on crystalline organic and inorganic solids. *J. Geophys. Res.,* **111,** D12204, doi:10.1029/2005JD006664.

Stith, J. L., C. H. Twohy, P. J. DeMott, D. Baumgardner, T. Campos, R. Gao, and J. Anderson, 2011: Observations of ice nuclei and heterogeneous freezing in a Western Pacific extratropical storm. *Atmos. Chem. Phys.,* **11,** 6229–6243.

Sullivan, R. C., L. Miambres, P. J. DeMott, A. J. Prenni, C. M. Carrico, E. J. T. Levin, and S. M. Kreidenweis, 2010a: Chemical processing does not always impair heterogeneous ice nucleation of mineral dust particles. *Geophys. Res. Lett.,* **37,** L24805, doi:10.1029/2010GL045540.

——, and Coauthors, 2010b: Irreversible loss of ice nucleation active sites in mineral dust particles caused by sulphuric acid condensation. *Atmos. Chem. Phys.,* **10,** 11 471–11 487, doi:10.5194/acp-10-11471-2010.

Twohy, C., and Coauthors, 2010: Relationships of biomass burning aerosols to ice in orographic wave clouds. *J. Atmos. Sci.,* **67,** 2437–2450.

Vali, G., 2008: Repeatability and randomness in heterogeneous freezing nucleation. *Atmos. Chem. Phys.,* **8,** 5017–5031, doi:10.5194/acp-8-5017-2008.

——, M. Chistensen, R. W. Fresh, E. L. Galyan, L. R. Maki, and R. C. Schnell, 1976: Biogenic ice nuclei. Part II: Bacterial sources. *J. Atmos. Sci.,* **33,** 1565–1570.

Virtanen, A., and Coauthors, 2010: An amorphous solid state of biogenic secondary organic aerosol particles. *Nature,* **467,** 824–827, doi:10.1038/nature09455.

Vrbka, L., and P. Jungwirth, 2006: Homogeneous freezing of water starts in the subsurface. *J. Phys. Chem.,* **110B,** 18 126–18 129, doi:10.1021/jp064021c.

Wagner, R., O. Möhler, H. Saathoff, M. Schnaiter, and T. Leisner, 2011: New cloud chamber experiments on the heterogeneous ice nucleation ability of oxalic acid in the immersion mode. *Atmos. Chem. Phys.,* **11,** 2083–2110.

Weber, R. J., and Coauthors, 2007: A study of secondary organic aerosol formation in the anthropogenic-influenced southeastern United States. *J. Geophys. Res.,* **112,** D13302, doi:10.1029/2007JD008408.

Welti, A., F. Luond, O. Stetzer, and U. Lohmann, 2009: Influence of particle size on the ice nucleating ability of mineral dusts. *Atmos. Chem. Phys.,* **9,** 6705–6715.

——, F. Lüönd, Z. A. Kanji, O. Stetzer, and U. Lohmann, 2012: Time dependence of immersion freezing. *Atmos. Chem. Phys. Discuss.,* **12,** 12 623–12 662.

Wiedinmyer, C., R. M. Bowers, N. Fierer, E. Horanyi, M. Hannigan, A. G. Hallar, I. McCubbin, and K. Baustian, 2009: The contribution of biological particles to observed particulate organic carbon at a remote high altitude site. *Atmos. Environ.,* **43,** 4278–4282.

Wilson, T. W., and Coauthors, 2012: Glassy aerosols with a range of compositions nucleate ice heterogeneously at cirrus temperatures. *Atmos. Chem. Phys. Discuss.,* **12,** 8979–9033, doi:10.5194/acpd-12-8979-2012.

Yankofsky, S. A., Z. Levin, T. Bertold, and N. Sandlerman, 1981: Some basic characteristics of bacterial freezing nuclei. *J. Appl. Meteor.,* **20,** 1013–1019.

Zaveri, R. A., J. C. Barnard, R. C. Easter, N. Riemer, and M. West, 2010: Particle-resolved simulation of aerosol size, composition, mixing state and the associated optical and cloud condensation nuclei activation properties in an evolving urban plume. *J. Geophys. Res.,* **115,** D17210, doi:10.1029/2009JD013616.

Zimmermann, F., S. Weinbruch, L. Schütz, H. Hofmann, M. Ebert, K. Kandler, and A. Worringen, 2008: Ice nucleation properties of the most abundant mineral dust phases. *J. Geophys. Res.,* **113,** D23204, doi:10.1029/2008JD010655.